A reassessment of the distinctiveness of dryopithecine genera from the Iberian Miocene based on enamel-dentine junction geometric morphometric analyses

Clément Zanolli[a,*], Florian Bouchet[b], Josep Fortuny[b], Federico Bernardini[c,d], Claudio Tuniz[d], David M. Alba[b,*]

[a] *Univ. Bordeaux, CNRS, MCC, PACEA, UMR 5199, F-33600 Pessac, France*

[b] *Institut Català de Paleontologia Miquel Crusafont, Universitat Autònoma de Barcelona, Edifici ICTA-ICP, c/ Columnes s/n, Campus de la UAB, 08193 Cerdanyola del Vallès, Barcelona, Spain*

[c] *Department of Humanistic Studies, Università Ca'Foscari, Venezia, Italy*

[d] *Multidisciplinary Laboratory, 'Abdus Salam' International Centre for Theoretical Physics, Via Beirut 31, 34151 Trieste, Italy*

*Corresponding authors.

E-mail addresses: clement.zanolli@gmail.com (C. Zanolli); david.alba@icp.cat (D.M. Alba).

A reassessment of the distinctiveness of dryopithecine genera from the Iberian Miocene based on enamel-dentine junction geometric morphometric analyses

Abstract

A vast diversity of catarrhines primates has been uncovered in the Middle to Late Miocene (12.5–9.6 Ma) of the Vallès-Penedès basin (northeastern Spain), including several hominid species (*Pierolapithecus catalaunicus, Anoiapithecus brevirostris, Dryopithecus fontani, Hispanopithecus laietanus*, and *Hispanopithecus crusafonti*) plus some remains attributed to '*Sivapithecus*' *occidentalis* (of uncertain taxonomic validity). However, *Pierolapithecus* and *Anoiapithecus* have also been considered junior synonyms of *Dryopithecus* by some authors, which entail a lower generic diversity and an inflated intrageneric variation of the latter genus. Since the distinction of these taxa partly relies on dental features, the detailed and quantitative analysis of tooth shape might help disentangling the taxonomic diversity of these Miocene hominids. Using diffeomorphic surface matching and three-dimensional geometric morphometrics, we investigate the enamel-dentine junction shape (which is a reliable taxonomic proxy) of these Miocene hominids, with the aim of investigating their degree of intra- and intergeneric variation compared with that of extant great ape genera. We conducted statistical analyses, including between-group principal component analyses, canonical variate analyses, and permutation tests, to investigate whether the individual and combined (i.e., *Dryopithecus* s.l.) variation of the extinct genera exceeds that of the extant great apes. Our results indicate that *Pierolapithecus*, *Anoiapithecus*, *Dryopithecus*, and *Hispanopithecus* show morphological differences of enamel-dentine junction shape relative to the extant great apes that are consistent with their attribution to different genera. Specifically, the variation displayed by the Middle Miocene taxa combined exceeds that of extant great ape genera, thus undermining the single-

genus hypothesis. '*Sivapithecus*' *occidentalis* specimens fall close to *Dryopithecus* but in the absence of well-preserved comparable teeth for *Pierolapithecus* and *Anoiapithecus*, their taxonomic attribution remains uncertain. Among the *Hispanopithecus* sample, IPS1802 from Can Llobateres stands out and might either be an outlier in terms of morphology, or represent another dryopithecine taxon.

Keywords: *Anoiapithecus*; *Dryopithecus*; *Hispanopithecus*; *Pierolapithecus*; Hominoidea; Spain

1. Introduction

Over the past two decades, discoveries in various Middle to Late Miocene localities of the Vallès-Penedès Basin (NE Iberian Peninsula; Casanovas-Vilar et al., 2016a) have revealed a previously unsuspected (e.g., see Andrews et al., 1996) high diversity of primates (Alba, 2012; Marigó et al., 2014; Alba et al., 2017, 2022), including multiple small-bodied catarrhines (Moyà-Solà et al., 2001; Alba et al., 2010a, 2012a, 2015; Alba and Moyà-Solà, 2012a) as well as fossil great apes (Moyà-Solà et al., 2004, 2009a, 2009b; Alba et al., 2011, 2012a; Alba and Moyà-Solà, 2012b). The presence of fossil catarrhines in the NE Peninsula has been related to the moister and more forested environments than elsewhere in Iberia during the late Aragonian and Vallesian, being more similar to those from France and Central Europe (ca. 12.6–8.9 Ma; Casanovas-Vilar et al., 2008, 2016a, 2016b; Alba, 2012; Marmi et al., 2012; Alba et al., 2018). In turn, the recognition of a greater diversity than expected mainly stems from the large sampling effort devoted during the last couple decades to Middle Miocene sites (Alba, 2012; Alba et al., 2017, 2022), which led to the realization that different dryopithecine genera were recorded in the Middle and Late Miocene of Europe (Moyà-Solà et al., 2009a; Begun, 2009; Alba, 2012), and has been recently substantiated by recent discoveries elsewhere in Europe (Böhme et al., 2019).

While there is consensus that Late Miocene dryopithecines belong to different genera than *Dryopithecus* (Moyà-Solà et al., 2009a; Begun, 2009; Alba, 2012), the distinctiveness of the Middle Miocene genera *Pierolapithecus* and *Anoiapithecus* from *Dryopithecus* has been challenged by Begun and coauthors (Begun, 2009; Begun et al., 2012), who, based on various similarities (reduced maxillary sinus and resemblances in overall dental morphology), concluded that *Pierolapithecus* and *Anoiapithecus* are likely junior subjective synonyms of *Dryopithecus* (i.e., genus names subsequently established based on different type specimens that, in the authors' opinion, do not warrant a distinction at the genus rank). The distinction of these three genera is mostly based on cranial differences (such as the presence of a frontal sinus, the position of the zygomatic root, or the degree of prognathism) coupled with more subtle dental differences (Moyà-Solà et al., 2004, 2009a, 2009b; Alba, 2012; Pérez de los Ríos et al., 2012, 2013; Alba et al., 2013, 2020; Fortuny et al., 2021). In turn, the postcranial evidence available indicates multiple differences between *Pierolapithecus* and the Late Miocene *Hispanopithecus*, but the more scanty evidence available for *Dryopithecus* and the absence of postcranial remains for *Anoiapithecus* do not enable reliable conclusions for these Middle Miocene dryopithecines (Moyà-Solà et al., 2004, 2009a; Almécija et al., 2007, 2009; Alba et al. 2010b, 2011, 2012b; Pina et al., 2012, 2019).

Previous analyses of the internal dental structure showed that *Dryopithecus* has proportionally thin enamel, as in the African great apes, while *Pierolapithecus* and *Anoiapithecus* display moderately thick enamel, similar to *Pongo* (Alba et al., 2010b, 2012a, 2020; Fortuny et al., 2021). In addition, some distinctive features were described on the outer enamel surface (OES) between *Pierolapithecus* and *Dryopithecus* (including thick and inflated crests, secondary enamel folds, and cusp base morphology; Alba et al., 2013, 2020; Pérez de los Ríos et al., 2013) that are not visible at the level of the enamel-dentine junction (EDJ), probably due to differences

in enamel thickness between the two genera (Fortuny et al., 2021). The external occlusal morphology and enamel thickness stem from the evolutionary interplay between functional/adaptive factors and strict control mechanisms of the morphogenetic program, and they respond relatively quickly in evolutionary time to dietary/ecological changes (reviewed in Zanolli et al., 2017). Conversely, the EDJ is the developmental precursor of crown shape and is more conservative than the enamel in evolutionary terms (i.e., reflecting macrevolutionary vs. microevolutionary changes, respectively; Korehof, 1961; Olejniczak et al., 2004; Skinner et al., 2008), carrying a marked phylogenetic signal in its shape (Zanolli et al., 2022b). The EDJ is recognized as a reliable taxonomic proxy to distinguish extinct and extant hominid taxa (e.g., Skinner et al., 2008, 2009; Macchiarelli et al., 2013; Fornai et al., 2015; Zanolli et al., 2015, 2019, 2022a; Pan et al., 2016, 2020). A number of traits were identified on the EDJ of *Pierolapithecus* maxillary molars that differ from *Dryopithecus* (deeper trigon basin, higher and straighter crista obliqua, lingual dentine horns mesiodistally aligned, less cervical buccolingual waisting, less developed lingual cingulum; Fig. 1A) and from *Anoiapithecus* (shallower and less restricted mesial fovea, M^1 and M^2 hypocone dentine horn less lingually situated relative to that of the protocone, markedly less buccolingually waisted cervix, and more weakly developed lingual cingulum; Fig. 1A; Fortuny et al., 2021).

The lower dentition of *Pierolapithecus* is unknown and most of the lower molars of *Anoiapithecus* are either not well preserved or worn, which complicates the diagnosis of isolated teeth or dentognathic fragments found in the Middle Miocene sites of the Vallès-Penedès Basin. In particular, two specimens are currently attributed to '*Sivapithecus*' *occidentalis* species inquirenda (Alba et al., 2020; Fortuny et al., 2021): IPS1826+IPS1827 (holotype), including the M_2 and M_3 of a single individual; and IPS41734, a mandibular fragment with M_2. The taxonomic allocation of the holotype specimen has varied among authors throughout the years, but most

recently Alba et al. (2020) considered it a species inquirenda because the lack of suitable material to compare it with other taxa makes it impossible to determine its taxonomic attribution with certainty (i.e., it is "a species of doubtful identity needing further investigation;" ICZN, 1999: Glossary). The three molars of '*S.*' *occidentalis* exhibit thick enamel, excluding the possibility that they belong to *Dryopithecus* (Alba et al., 2020; Fortuny et al., 2021). They also show thinner enamel than the two species of *Hispanopithecus*, as well as a combination of different morphological characteristics at the EDJ (including more centrally tilted metaconid dentine horns, with a well-developed metaconulid dentine horn; Fig. 1B). '*Sivapithecus*' *occidentalis* is a senior subjective synonym of either *Pierolapithecus catalaunicus* or *Anoiapithecus brevirostris* (i.e., '*S.*' *occidentalis* was established, based on a different type specimen, before the other species, and it would thus take precedence if it was eventually considered that it is conspecific with either of them). This is indeed likely, given that the holotypes of these species come from the same area and a very restricted time span of less than 100 kyr (Alba et al., 2022), but currently available data from the occlusal surface are insufficient to reach a definitive conclusion in this regard (Alba et al., 2020; Fortuny et al., 2021).

To further investigate the taxonomic diversity of Iberian dryopithecines and to test whether the genera currently recognized (*Pierolapithecus*, *Anoiapithecus*, *Dryopithecus*, and *Hispanopithecus*) can be readily distinguished on dental grounds, we conducted diffeomorphic surface matching and three-dimensional (3D) geometric morphometrics of the EDJ shape. We also evaluated the degree of intra- and intergeneric variation of these dryopithecine genera in comparison with that of extant great ape genera.

2. Materials and methods

2.1. Dryopithecine specimens and extant comparative sample

The Miocene dryopithecine sample includes 45 molars from 25 specimens from the Vallès-Penedès and Seu d'Urgell basins (Catalonia, Spain), housed at the Institut Català de Paleontologia Miquel Crusafont. Details of the µCT scans, segmentation process, and description of the EDJ of these specimens are reported in Fortuny et al. (2021). The surface models of the EDJ of these dryopithecine molars are available on MorphoSource (https://www.morphosource.org; the list of the digital object identifiers for each specimens can be found in Supplementary Online Material [SOM] Table S1). Four molars belonging to three specimens attributed to *Dryopithecus fontani* from Saint-Gaudens (type locality), in France, were used as reference material. The *D. fontani* specimens are curated at the Muséum de Bordeaux. More information on the fossil samples is available in SOM Table S1. One specimen, IPS1816, was previously regarded as an M_2, but based on root morphology as shown by the µCT scan (especially that of the mesially-located tooth that resembles more a P_4 root; SOM Fig. S1), and in agreement with the general crown morphology, it is more likely to represent an M_1.

The extant comparative sample includes 60 molars per genus (10 upper and 10 lower teeth per molar position and per genus) for *Pan*, *Gorilla*, and *Pongo* (SOM Table S2). For each molar position, because of the limited availability of extant comparative material, the antimeres of some specimens were sometimes used to reach 10 teeth/genus. It is also recommendable to include antimeres for the extant species because it cannot be excluded that some of the right and left isolated molars from the same position and fossil locality belong to a single individual. To represent as much as possible the extant intrageneric variation, specimens of both sexes, from various geographic areas, and of different species (with two species of *Pan*—*Pan troglodytes* and *Pan paniscus*—and two species of *Pongo*—*Pongo pygmaeus* and *Pongo abelii*) were included (SOM Table S2).

2.2. Geometric morphometric analyses of the enamel-dentine junction

We used a diffeomorphic surface matching (DSM) approach to analyze EDJ shape (Durrleman et al., 2012, 2014). Diffeomorphic surface matching analyses can capture the taxonomically relevant aspects of EDJ morphology (Beaudet et al., 2016; Zanolli et al., 2018, 2022a; Braga et al., 2019), including both prominent features (such as the dentine horns and marginal crests) and more subtle features (like the protostylid and occlusal basin morphology), and thus improves on traditional (semi)landmark-based geometric morphometric analyses (Zanolli et al., 2018; Braga et al., 2019; Urciuoli et al., 2020, 2021a). This landmark-free, mesh-based approach relies on the construction of average surface models, and the difference between surfaces is interpreted as the amount of deformation needed to align them by using diffeomorphic shape matching (Glaunès and Joshi, 2006; Durrleman et al., 2014). The deformations between surfaces are mathematically modeled as smooth and invertible functions (i.e., diffeomorphisms). From a set of surfaces, an atlas of surfaces is created. The method estimates an average object configuration or mean shape from a collection of object sets (here the EDJ surfaces) and computes the deformations from the mean shape to each specimen. In addition, a set of initial control points located near its most variable parts, and a set of momenta parameterizing the deformations of the mean shape to each specimen are estimated (Durrleman et al., 2012).

For each tooth position, the EDJ surfaces decimated to 50,000 polygons were manually oriented, then superimposed using the rigid and uniform scale option of the 'Align Surfaces' module in Avizo v. 7.0 (FEI Visualization Sciences Group, Hillsboro). This was done by minimizing the root mean square distance between the points of each specimen to corresponding points on the reference surface using an iterative closest-point algorithm. We used Deformetrica v. 4.3 software (Bône et al., 2018) to generate a global mean shape with a set of diffeomorphisms relating the global mean shape to each individual and the output (control points and deformation

momenta) used to perform the statistical analyses to explore the EDJ shape variation and to classify the data. Deformations were computed at the IN2P3 Computing Center (Lyon, France). The output data were imported into R v. 4.1.3 (R Core Team, 2022) with the package 'RToolsForDeformetrica' v. 0.1 (Dumoncel, 2021). Using the packages 'ade4' v. 1.7-6 (Dray and Dufour, 2007) and 'Morpho' v. 2.8 (Schlager, 2020) for R, we first computed principal component analyses (PCAs), followed by between-group PCAs (bgPCAs) based on the deformation moments and using the following three groups assigned with equal prior probabilities: *Pan*, *Gorilla,* and *Pongo*. The Iberian Miocene specimens were then projected a posteriori into the bgPCA morphospace. We followed the recommendations of Cardini and Polly (2020) by computing cross-validated bgPCAs (cv-bgPCAs) to ensure that group discrimination is not spurious using the package 'Morpho'. We also performed cross-validated canonical variates analyses (CVAs) using the same groups as for the bgPCAs using the R package 'Morpho'. Since CVA computation requires the number of variables to be much smaller than the number of specimens, we computed the CVAs based on a subset of the first principal component (PC) scores showing the highest degree of correct classification (screening the correct classification results and selecting the minimum number of PC scores enabling to reach the optimum of correct classification; Hastie et al., 2009). Between three and six PC scores representing ca. 60 to 76% of the total variance were selected for CVA analyses. This choice of PC scores subset is a compromise between including a sufficient proportion of overall shape variation and limiting the number of variables to avoid unrealistic and unstable levels of discrimination (Skinner et al., 2009). We also assessed the structuration of data and results of the multivariate analyses to test that group separation is not spurious (Cardini and Polly, 2020). The amount of variance (r^2) explained by group differences in the raw shape data was estimated by computing a permutational multivariate analysis of variance (PERMANOVA; 1000 permutations) based on

the Euclidean distance between the means and implementing a Holm correction using the R packages 'vegan' v. 2.5-7 (Oksanen et al., 2020) and 'pairwiseAdonis' v. 0.3 (Martínez Arbizu, 2020).

We computed the Euclidian distances (EDs) between specimens for the bgPCA and CVA scores to assess intra- and intergeneric variation in the comparative sample (for an example with Procrustes distances, see Spoor et al., 2015). Distances for bgPCA and CVA scores were computed between each specimen of the same genus (i.e., intrageneric variation) for both extant and extinct genera, and also between specimens of samples combining two or more different dryopithecine genera (i.e., intergeneric variation). To ensure that these analyses were not biased by the small sizes of the fossil samples we further performed permutation tests. For intrageneric variation analyses, fossil samples were restricted to the specimens available for each genus. For intergeneric variation analyses, fossil samples included specimens from two or more genera to test the hypotheses that *Pierolapithecus* and *Anoiapithecus* might be junior synonyms of *Dryopithecus* (Begun, 2009; Begun et al., 2012) and that '*Sivapithecus*' *occidentalis* species inquirenda (Alba et al., 2020; Fortuny et al., 2021) might be a senior synonym of *P. catalaunicus* or *A. brevirostris*. For each fossil sample, the ED based on the scores of the two first bgPCs (representing more than 90–95% of the variance) and CVs (representing 100% of the variance) was computed for each pair of specimens and the average ED was calculated. For each extant genus, we generated all the possible combinations (permutations) of specimens with the same sample size as the fossil sample of interest, and average ED for each set of permutations was calculated as explained above. Average ED for each fossil sample was then compared with the distribution of average EDs for the corresponding extant set of permutations. The probability of each fossil sample displaying a lower variation than each extant genus was computed by dividing the number of extant permutations with a higher or equal average ED than that of the fossil

sample by the total number of extant permutations. The null hypothesis that a given fossil sample does not exceed the variation seen within an extant genus was rejected when the aforementioned probability (interpreted as a *p*-value) was lower than 5% ($p < 0.05$). For intergeneric comparisons (i.e., including specimens from multiple dryopithecine genera), rejecting the null hypothesis would support the existence of more than a single genus (unless more variable than extant ones), whereas failure to reject the null hypothesis would be compatible with a single genus (but would not reject the presence of multiple genera).

3. Results

Comparisons between bgPCA and cv-bgPCA plots show a similar degree of discrimination between *Pan*, *Gorilla*, and *Pongo* (Fig. 2; SOM Fig. S2). Results of the PERMANOVA based on the raw data confirm the high level of discrimination between the three groups for all tooth positions (SOM Table S3). Results of the CVA are similar to those of bgPCA (Figs. 2 and 3). The EDJs of both maxillary and mandibular molars of each extant genus are equally correctly classified, but M1s and M2s show a greater taxonomic discriminatory power than M3s (SOM Tables S3 and S4). Correct classification for each group and overall classification resulting from the cv-bgPCA and CVA are reported in SOM Table S4. Collectively, bgPCA, cv-bgPCA, and CVA analyses are consistent with each other and confirm that the groups observed in the bgPCA and CVA are not spurious. In both the bgPCA and CVA, the first component separates taxa based on EDJ height (and in particular dentine horn elevation), with *Gorilla* showing the highest dentine horns, *Pongo* the lowest, and *Pan* being intermediate (Figs. 2 and 3). The second component tends to discriminate the more centrally-positioned dentine horns of *Pongo* and *Gorilla* from those of *Pan*.

The bgPCA and CVA plots show that the Miocene specimens are distributed in a distinct part of the morphospace, generally near *Pongo*, but sometimes intermediate between *Pongo* and *Pan*, and less frequently close to *Pan* (Figs. 2 and 3). In particular, the M^2s of *Anoiapithecus* and *Pierolapithecus*, as well as some M^2s and M_2s of *Hispanopithecus*, tend to be closer to the morphology of *Pan* than to that of the other extant great apes. This is supported by typicality probabilities, even if for a number of dryopithecine specimens, the highest value is lower than 0.05, indicating that they are outside the variation of the extant genera (Table 1). Despite the limited sample size of the Miocene hominids, the teeth belonging to the same genus tend to cluster together for most tooth positions (only for the M^3, the range of *Hispanothecus* specimens is relatively large, similar to that of *Pongo*). While the distribution of the various Miocene specimens does not exceed that of the extant great apes for the first molars (comparable to the extent of variation of *Pongo*), second and third molars are more widely scattered than they are in the extant great ape genera.

When investigating the Euclidian distances between specimens, the intrageneric variation of extant apes is limited to a similar range for each extant great ape genus in both the bgPCA (Fig. 4) and CVA (Fig. 5). *Gorilla* and *Pan* are generally less variable in EDJ shape than *Pongo*. *Hispanopithecus* M^3 and M_2 EDJ vary the most among the fossil genera, but they are within a similar range to that of *Pongo* (Figs. 4C and 5C, E), except in the M_2 bgPCA morphospace, where *Hispanopithecus* shows a higher degree of variation than each extant genus (Fig. 4E). For the M^2 position, *Dryopithecus* appears to differ more from both *Anoiapithecus* and *Pierolapithecus* than the two latter genera from one another (Figs. 4B and 5B). *Pierolapithecus* M^3 EDJ differs from that of the other Miocene genera due to the highly mesiodistally compressed crown morphology (Fortuny et al., 2021: Fig. 4C). '*Sivapithecus*' *occidentalis* M_2 and M_3 EDJ differ more from *Hispanopithecus* than *Dryopithecus*.

Permutation tests based on the bgPCA and CVA scores confirm that the Miocene genera exhibit a degree of molar EDJ intrageneric variation that is generally not greater than that of extant great ape genera (Table 2). The only exceptions are the *Hispanopithecus* M^3s (which vary more than those of *Gorilla* and *Pan* but not *Pongo*) and M_2s (which show variation even exceeding the range of the three extant great ape genera (except *Pongo* based on the bgPCA results). By contrast, when the permutation tests are repeated by mixing teeth of different Middle Miocene taxa, the results are somewhat different, as in multiple instances their variation exceeds that of one or more extant great ape genera (Table 3). Fossil samples including *Anoitapithecus*, *Dryopithecus*, and *Pierolapithecus* are only available for the upper molars. The M^1 variation only surpasses that of *Gorilla* based on the bgPCA results, but M^3 variation exceeds that of both *Gorilla* and *Pan*, and M^2 variation exceeds that of all extant great ape genera. The results for the M^3 might be explained by a high degree of variation (as in *Hispanopithecus*, see above) but those for the M^2 support the presence of more than a single genus in the Middle Miocene sample. When intergeneric variation is evaluated by mixing two extinct genera at a time (Table 3), permutation tests indicate that the single-genus hypothesis can be rejected for *Anoiapithecus–Dryopithecus* based on the M^2 and for *Dryopithecus–Pierolapithecus* (and *Anoitapithecus–Pierolapithecus* except when compared with *Pongo* in the bgPCA results) based on the M^3. Permutation tests based on lower molars are of less utility because they are unknown for *Pierolapithecus* and only the M_1 is available for *Anoiapithecus*, but they indicate that the variation of composite samples including *Dryopithecus* and '*S.*' *occidentalis* do not exceed that of extant great ape genera for either the M_2 or the M_3.

4. Discussion and conclusions

The taxonomic diversity of Iberian dryopithecines has been discussed frequently in the last decades, notably due to the increasing number of discoveries in the various localities of the Vallès-Penedès Basin (see review in Alba, 2012). There is a general consensus that the Middle Miocene genera *Pierolapithecus*, *Anoiapithecus*, and *Dryopithecus* differ from the Late Miocene *Hispanopithecus* and *Rudapithecus* (Moyà-Solà et al., 2009a; Begun, 2009; Alba, 2012; Almécija et al., 2021; Fortuny et al., 2021; Pugh, 2022), being classified into two distinct tribes (Dryopithecini and Hispanopithecini, respectively; Alba, 2012). However, the distinctiveness of the former three genera, which are roughly coeval (Casanovas-Vilar et al., 2011; Alba et al., 2017), has been questioned on several occasions, often based on arguments involving dental morphology (Begun, 2007, 2009, 2010; Begun et al., 2012). For example, *Pierolapithecus* and *Dryopithecus* were described as sharing the large canines, short premolars, partial cingulum of the molars, and smaller M1 relative to M2, and *Anoiapithecus* was also regarded as sharing similar features (Begun, 2009; Begun et al., 2012). However, it is widely recognized that dryopithecines are dentally conservative and that the distinction among different genera is largely based on cranial and postcranial features (e.g., Alba, 2012; Almécija et al., 2021), even though some dental differences have previously been noticed (Alba et al., 2013; Pérez de los Ríos et al., 2013). The overall degree of similarity within the Iberian dryopithecine genera is likely related to their short stratigraphic ranges. Specimens from Abocador de Can Mata span from ~12.4–11.9 Ma (Alba et al., 2017, 2022), and the *Hispanopithecus* remains range between ~10.5 and 9.5 Ma (Alba et al., 2018). These ranges are shorter than the molecular divergence dates of the extant species of *Pan* (~2 Myr; Prüfer et al., 2012), suggesting that temporal trends are unlikely to play a substantial role in inflating the variation of these previously recognized dryopithecine genera.

Previous analyses of the molar structural organization in the Iberian dryopithecines, including the detailed description of OES and EDJ morphology, as well as enamel thickness,

supported the discrimination of *Pierolapithecus*, *Anoiapithecus*, *Dryopithecus*, and *Hispanopithecus* as distinct genera (Alba et al., 2010, 2013; Fortuny et al., 2021). Our results of the 3D geometric morphometric analyses of the EDJ are also in agreement with these former studies. As shown by the bgPCA, CVA, and Euclidian distance plots (Figs. 2–5), the distribution of the Iberian dryopithecine genera exceeds the variation of each extant great ape genus, especially for the M2 and M3 positions, while M1s tend to be less variable (both in fossil and extant genera). This is confirmed by the permutation tests based on the upper molars, which reject the single-genus hypothesis and rather support the distinctiveness of *Pierolapithecus* and *Anoiapithecus* from one another as well as when compared with *Dryopithecus*.

It has been argued that the I^1 and M^3 of *Pierolapithecus* closely resemble those of *Dryopithecus* from La Grive (Begun, 2009; Begun et al., 2012). However, other authors have noted that the La Grive incisor differs in several respects from that of *Pierolapithecus* (and *Hispanopithecus*), whereas the upper molar (reinterpreted as a female M^1) more closely resembles *Dryopithecus* in crown height (Pérez de los Ríos et al., 2013). Regardless, the distance separating the EDJ of the only available M^3 of *Pierolapithecus* (IPS21350) from that of *Dryopithecus* (IPS35026) largely exceeds the intrageneric variation of the three extant great ape genera and, together with the permutation tests (Table 3), contradict the single-genus hypothesis. In addition, the *Dryopithecus* M^2 displays a more buccolingually compressed central basin relative to crown base and more lingually-placed hypocone than that of *Pierolapithecus* (Fig. 1A; see also Fortuny et al., 2021). *Anoiapithecus* and *Dryopithecus* M^2s are also well distinguished and the distance between specimens exceeds the degree of variation displayed by the three extant great ape genera (Table 3), mostly due to the more asymmetric and higher EDJ in the former (Figs. 2–5). These quantitative analyses support the distinction of these two taxa at genus rank and are in contradiction with the hypothesis that they are congeneric (Begun, 2009). It has also

been suggested that *Pierolapithecus* and *Anoiapithecus* are dentally very similar and may belong to the same genus (Begun, 2009; Begun et al., 2012). The differences between the EDJ of the molars of these two genera are more or less marked depending on tooth position. For the M^2, the EDJs of both taxa are morphologically quite similar, and the variation they express in the available sample does not exceed that of the extant great ape genera (Figs. 2–5). However, for the M^1 and M^3, these two dryopithecine genera are relatively distant in both the bgPCA and CVA (Figs. 2 and 3). In fact, *Pierolapithecus* and *Anoiapithecus* M^3 specimens are more distant from each other than the specimens of each extant hominid genus are in the bgPCA space (Fig. 4C), and their variation is only included within the intrageneric range of *Pongo* in the CVA (Fig. 5C), as indicated by the permutation tests (Table 3). In terms of morphology, as previously described (Fortuny et al., 2021), our results show that *Pierolapithecus* has more mesiodistal compressed EDJs (particularly for the M^3), with shorter and slightly more peripherally-placed dentine horns than *Anoiapithecus*. Even if the distinction between *Pierolapithecus* and *Anoiapithecus* is not as striking as that between *Pierolapithecus* and *Dryopithecus*, or between *Anoiapithecus* and *Dryopithecus*, the results of our geometric morphometric analyses of EDJ shape (in particular based on permutation tests for the M^3; Table 3) are consistent with the hypothesis that they represent different genera. These results are in further agreement with the previously described cranial differences between *Anoiapithecus* and *Pierolapithecus*, including prognathism (much more orthognathous facial profile in *Anoiapithecus*), presence vs. absence of a frontal sinus, thinner vs. thicker enamel, and more vs. less downward inclination of the zygomatic root (Moyà-Solà et al., 2009b; Fortuny et al., 2021).

The taxonomic status of the M_2s and M_3 currently assigned to '*S.*' *occidentalis* is also unclear as they have been suggested to belong to either *P. catalaunicus* or *A. brevirostris* (Alba et al., 2020). The permutation tests indicate that an attribution to *Dryopithecus* cannot be discounted

(Table 3), but the lack of mandibular remains for *Pierolapithecus* and the fragmentary state of the *Anoiapithecus* specimen IPS43000 M_2 (and absence of M_3) preclude a more conclusive assessment. The EDJ shape analyses conducted here show that the three '*S.*' *occidentalis* molars are closer to *Dryopithecus* than *Hispanopithecus* (IPS1826+1827 and IPS41734). These analyses also suggest that *Pierolapithecus* EDJ is closer to that of *Dryopithecus* for the M^1 and M^2 than *Anoiapithecus* is (Figs. 2A, B and 3A, B). However, the three '*S.*' *occidentalis* molars exhibit thick enamel (3D relative enamel thickness [3D RET]: 17.16–20.63), overlapping with the range of *Pierolapithecus* (3D RET: 13.24–18.14), whereas both *Dryopithecus* (3D RET: 10.96–12.81) and *Anoiapithecus* show thin enamel (3D RET: 11.40–14.26; Fortuny et al., 2021). If IPS1826+1827 and IPS41734 belonged to one of the taxa recognized here, both signals of the EDJ and enamel thickness would suggest that they would more likely represent *Pierolapithecus* than *Anoiapithecus*. Nevertheless, no definitive attribution can be given to these fossils until more mandibular remains belonging to the latter two genera are recovered and analyzed.

The Late Miocene *Hispanopithecus* was considered as a junior subjective synonym of *Dryopithecus* for years (e.g., Harrison, 1991; Andrews et al., 1996), until the genus was resurrected (Begun, 2009; Moyà-Solà et al., 2009a) for both *Hispanopithecus laietanus* and *Hispanopithecus crusafonti*. The later species, which includes the samples from Can Ponsic 1 and Teuleria del Firal, is classified in *Hispanopithecus* based on dental morphology because it shows some derived features with *H. laietanus*, coupled with a number of autapomorphic traits such as buccolingually broader upper molars (Begun, 1992; Begun, 2002, Alba, 2012). In terms of morphology of the molar EDJ, the dentine horns of *Hispanopithecus* are more peripherally located than in *Dryopithecus* (Fig. 1; Fortuny et al., 2021). Shape analyses of the EDJ show that the specimens attributed to *Hispanopithecus* plot close to *Dryopithecus*, and to a lesser extent to *Anoiapithecus* (Figs. 2–5). The most surprising result of these analyses regards the high degree of

variability of *Hispanopithecus* M_2s. Even though two species are included in the genus (i.e., *H. crusafonti* and *H. laietanus*), they vary more than the extant great ape genera as represented in this study (Figs. 2E, 3E, 4E, and 5E), as confirmed by permutation tests (Table 2). We acknowledge that the comparative sample of extant hominids included in this study might underestimate the actual degree of variation of each genus, but the same is true for the fossil samples. In addition, despite its limited size, the sample extant great apes represents male and female individuals of different species of *Pan* and *Pongo* (and possibly of *Gorilla* too, even though there is no contextual information for some specimens). For these reasons, the extant hominid sample is assumed to be representative of each genus, even though it likely underestimates their real range of variation due to the limits of sample size. For example, at least for *Pongo* M_2s, two species (*P. pygmaeus* and *P. abelii*) are represented (SOM Table S2) and they are much less variable than those of *Hispanopithecus*. The high variability of the latter genus is mostly driven by IPS1082, which falls farther from the other four *Hispanopithecus* M_2s. This could be interpreted in two different ways: 1) the M_2 of IPS1802 is an outlier in terms of morphology, but belongs to *Hispanopithecus*; 2) IPS1802 belongs to another genus, but is closely related to *Hispanopithecus*. The small dimensions of this specimen compared with the other *H. laietanus* lower molars (Alba et al., 2012c) could also indicate that it belongs to a female of *Hispanopithecus*, but it would mean that sexual dimorphism in molar shape (especially at the EDJ level) would be higher than in extant great apes and the other dryopithecines, which is unlikely. It is noteworthy that IPS1802 (a mandibular fragment with M_1–M_3) was planned to be the holotype of *Rahonapithecus sabadellensis*, a nomen dubium because Crusafont-Pairó and Hürzeler (1961, 1969) never described them (Fortuny et al., 2021, and references therein). Pickford (2012) considered this specimen (as well as the holotype of '*S.*' *occidentalis*) to belong to *Neopithecus brancoi*, which is here considered a nomen dubium (see also Moyà-Solà et al.,

2009a; Begun, 2015; Alba et al., 2020). Nevertheless, this specimen hints at the possibility that some of the Middle Miocene genera recorded at Abocador de Can Mata persisted into the Vallesian and co-occurred with *Hispanopithecus* at Can Llobateres.

The phylogenetic relationships of the Iberian Miocene dryopithecines are still debated (see review in Almécija et al., 2021). *Pierolapithecus*, *Anoiapithecus*, and *Dryopithecus* have been either considered as stem hominids (Moyà-Solà et al., 2004, 2009b; Pugh, 2022), stem pongines, (Pérez de los Ríos et al., 2012) or hominines (Begun, 2010). In turn, *Hispanopithecus* has been variably considered a stem pongine (Moyà-Solà and Köhler, 1995), a stem hominine (Begun et al., 2012), or a stem hominid (Moyà-Solà et al., 2009b). A recent cladistic analysis of Middle to Late Miocene hominoids based on 274 dental and skeletal traits found dryopithecines (excluding *Ouranopithecus*, *Graecopithecus*, and *Oreopithecus*) to be no more closely to hominines than to pongines and supported the Middle Miocene dryopithecins as being less derived than the Late Miocene hispanopithecins (Pugh, 2022). A study investigating the phylogenetic signal of the inner ear morphology in primates indicated that the hispanopithecin genera *Hispanopithecus* and *Rudapithecus* show closest affinities in vestibular morphology with *Pan* but also with the inferred morphology for the last common ancestors of crown hominines and crown hominids, suggesting that such morphology is plesiomorphic (Urciuoli et al., 2021b). Another study based on the EDJ of primate M_1s showed that this structure holds a very strong phylogenetic signal and can be used, in addition to the inner ear, to investigate evolutionary relationships (Zanolli et al., 2022b). Posterior probabilities computed for the dryopithecine specimens in the bgPCA and CVA of the present study indicate closer shape similarities with *Pongo* for most taxa and tooth positions, even if a few specimens are closer to *Pan* (Table 1). However, as in the case of the aforementioned inner ear similarities with *Pan*, the EDJ results cannot be taken as suggesting a closer phylogenetic link with pongines without a proper phylogenetic analysis evaluating the

polarity of change so as to discern if these features are primitive for hominids or derived for pongines. The study of the EDJ in other European dryopithecine taxa, such as *Rudapithecus* and *Danuvius* (Begun, 2009, 2015; Böhme et al., 2019), or specimens of doubtful taxonomic allocation (such as the holotype of *N. brancoi*), will be required to better understand the evolution of this group during the Miocene.

Acknowledgments

For access to comparative material, we sincerely thank P. Bayle, A. Beaudet, J. Braga, E. Gilissen, M. Landreau, A. Mazurier, N. Mémoire, R. Macchiarelli. We thank Sergio Llácer for image processing, and Sebastià Calzada for the loan of specimens housed at the MGSB. We gratefully acknowledge support from the CNRS/IN2P3 Computing Center (Lyon, France) for providing computing and data-processing resources needed for this work. This research benefited from the scientific framework of the University of Bordeaux's IdEx "Investments for the Future" program / GPR "Human Past". This paper is part of R+D+I projects PID2020-116908GB-I00, PID2020-117118GB-I00 and PID2020-117289GB-I00, funded by the Spanish Agencia Estatal de Investigación (MCIN/AEI/10.13039/501100011033/), as well as a Ramón y Cajal grant to J.F. (RYC2021-032857-I) financed by the Spanish Agencia Estatal de Investigación (MCIN/AEI/10.13039/501100011033) and the European Union “NextGenerationEU” / PRTR. Research has also been funded by the French CNRS, CERCA Programme/Generalitat de Catalunya, predoctoral fellowship (Agència de Gestió d’Ajuts Universitaris i de Recerca, Generalitat de Catalunya) to Fl.B., and the Regione Friuli-Venezia Giulia (ICTP/Elettra EXACT Project) in the frame of the SAPIENS Project funded by the Centro Fermi. J.F. and D.M.A. are members of consolidated research groups 2017 SGR 086 and 2017 SGR 116, respectively. Finally, we thank the co-Editor-in-Chief (Andrea Taylor), the Associate Editor, and three

anonymous reviewers for their comments that helped improve a previous version of this manuscript.

References

Alba, D.M., 2012. Fossil apes from the Vallès-Penedès Basin. Evol. Anthropol. 21, 254–269.

Alba, D.M., Moyà-Solà, S., 2012a. A new pliopithecid genus (Primates: Pliopithecoidea) from Castell de Barberà (Vallès-Penedès Basin, Catalonia, Spain). Am. J. Phys. Anthropol. 147, 88–112.

Alba, D.M., Moyà-Solà, S., 2012b. On the identity of a hominoid male upper canine from the Vallès-Penedès Basin figured by Pickford (2012). Estud. Geol. 68, 149–153.

Alba, D.M., Moyà-Solà, S., Malgosa, A., Casanovas-Vilar, I., Robles, J.M., Almécija, S., Galindo, J., Rotgers, C., Bertó Mengual, J.V., 2010a. A new species of *Pliopithecus* Gervais, 1849 (Primates: Pliopithecidae) from the Middle Miocene (MN8) of Abocador de Can Mata (els Hostalets de Pierola, Catalonia, Spain). Am. J. Phys. Anthropol. 141, 52–75.

Alba, D.M., Fortuny, J., Moyà-Solà, S., 2010b. Enamel thickness in Middle Miocene great apes *Anoiapithecus*, *Pierolapithecus* and *Dryopithecus*. Proc. R. Soc. B 277, 2237–2245.

Alba, D.M., Moyà-Solà, S., Almécija, S., 2011. A partial hominoid humerus from the middle Miocene of Castell de Barberà (Vallès-Penedès Basin, Catalonia, Spain). Am. J. Phys. Anthropol. 144, 365–381.

Alba, D.M., Moyà-Solà, S., Robles, J.M., Galindo, J., 2012a. Brief Communication: The oldest pliopithecid record in the Iberian Peninsula based on new material from the Vallès-Penedès Basin. Am. J. Phys. Anthropol. 147, 135–140.

Alba, D.M., Casanovas-Vilar, I., Almécija, S., Robles, J.M., Arias-Martorell, J., Moyà-Solà, S., 2012b. New dental remains of *Hispanopithecus laietanus* (Primates: Hominidae) from Can

Llobateres 1 and the taxonomy of Late Miocene hominoids from the Vallès-Penedès Basin (NE Iberian Peninsula). J. Hum. Evol. 63, 231–246.

Alba, D.M., Almécija, S., Casanovas-Vilar, I., Méndez, J.M., Moyà-Solà, S., 2012c. A partial skeleton of the fossil great ape *Hispanopithecus laietanus* from Can Feu and the mosaic evolution of crown-hominoid positional behaviors. PLoS One 7, e39617.

Alba, D.M., Fortuny, J., Pérez de los Ríos, M., Zanolli, C., Almécija, S., Casanovas-Vilar, I., Robles, J.M., Moyà-Solà, S., 2013. New dental remains of *Anoiapithecus* and the first appearance datum of hominoids in the Iberian Peninsula. J. Hum. Evol. 65, 573–584.

Alba, D.M., Almécija, S., DeMiguel, D., Fortuny, J., Pérez de los Ríos, M., Pina, M., Robles, J.M., Moyà-Solà, S., 2015. Miocene small-bodied ape from Eurasia sheds light on hominoid evolution. Science 350, aab2625.

Alba, D.M., Casanovas-Vilar, I., Garcés, M., Robles, J.M., 2017. Ten years in the dump: An updated review of the Miocene primate-bearing localities from Abocador de Can Mata (NE Iberian Peninsula). J. Hum. Evol. 102, 12–20.

Alba, D.M., Casanovas-Vilar, I., Furió, M., García-Paredes, I., Angelone, C., Jovells-Vaqué, S., Luján, A.H., Almécija, S., Moyà-Solà, S., 2018. Can Pallars i Llobateres: A new hominoid-bearing locality from the late Miocene of the Vallès-Penedès Basin (NE Iberian Peninsula). J. Hum. Evol. 121, 193–203.

Alba, D.M., Fortuny, J., Robles, J.M., Bernardini, F., Pérez de los Rios, M., Tuniz, C., Moyà-Solà, S., Zanolli, C., 2020. A new dryopithecine mandibular fragment from the middle Miocene of Abocador de Can Mata and the taxonomic status of '*Sivapithecus*' *occidentalis* from Can Vila (Vallès-Penedès Basin, NE Iberian Peninsula). J. Hum. Evol. 145, 102790.

Alba, D.M., Robles, J.M., Casanovas-Vilar, I., Beamud, E., Bernor, R.L., Cirilli, O., DeMiguel, D., Galindo, J., Llopart, I., Pons-Monjo, G., Sánchez, I.M., Vinuesa, V., Garcés, M., 2022. A

revised (earliest Vallesian) age for the hominoid-bearing locality of Can Mata 1 based on new magnetostratigraphic and biostratigraphic data from Abocador de Can Mata (Vallès-Penedès Basin, NE Iberian Peninsula). J. Hum. Evol. 70, 103237.

Almécija, S., Alba, D.M., Moyà-Solà, S., Köhler, M., 2007. Orang-like manual adaptations in the fossil hominoid *Hispanopithecus laietanus*: first steps towards great ape suspensory behaviours. Proc. R. Soc. B 274, 2375–2384.

Almécija, S., Alba, D.M., Moyà-Solà, S., 2009. *Pierolapithecus* and the functional morphology of Miocene ape hand phalanges: paleobiological and evolutionary implications. J. Hum. Evol. 57, 284–297.

Almécija, S., Hammond, A.S., Thompson, N.E., Pugh, K.D., Moyà-Solà, S., Alba, D.M., 2021. Fossil apes and human evolution. Science 372, eabb4363.

Andrews, P., Harrison, T., Delson, E., Bernor, R.L., Martin, L., 1996. Distribution and biochronology of European and Southwest Asian Miocene catarrhines. In: Bernor, R.L., Fahlbusch, V., Mittmann, H.-W. (Eds.), The Evolution of Western Eurasian Neogene Mammal Faunas. Columbia University Press, New York, pp. 168–207.

Beaudet, A., Dumoncel, J., Thackeray, J.F., Bruxelles, L., Duployer, B., Tenailleau, C., Bam, L., Hoffman, J., de Beer, F., Braga, J., 2016. Upper third molar internal structural organization and semicircular canal morphology in Plio-Pleistocene South African cercopithecoids. J. Hum. Evol. 95, 104–120.

Begun, D.R., 1992. *Dryopithecus crusafonti* sp. nov., a new Miocene hominoid species from Can Ponsic (Northeastern Spain). Am. J. Phys. Anthropol. 87, 291–309.

Begun, D.R., 2002. European hominoids. In: Hartwig, W.C. (Ed.), The Primate Fossil Record. Cambridge University Press, Cambridge, pp. 339–368.

Begun, D.R., 2007. Fossil record of Miocene hominoids. In: Henke, W, Tattersall, I, (Eds.), Handbook of Paleoanthropology. Springer Verlag, Heidelberg, pp. 921–977.

Begun, D.R., 2009. Dryopithecins, Darwin, de Bonis, and the European origin of the African apes and human clade. Geodiversitas 31, 789–816.

Begun, D.R., 2010. Miocene hominids and the origins of the African apes and humans. Ann. Rev. Anthropol. 39, 67–84.

Begun, D.R., 2015. Fossil record of Miocene hominoids. In: Henke, W., Tattersall, I. (Eds.), Handbook of Paleoanthropology. Springer-Verlag, Berlin, Heidelberg, pp. 1261–1332.

Begun, D.R., Nargolwalla, M.C., Kordos, L., 2012. European Miocene hominids and the origin of the African ape and human clade. Evol. Anthropol. 21, 10–23.

Böhme, M., Spassov, N., Fuss, J., Tröscher, A., Deane, A.S., Prieto, J., Kirscher, U., Lechner, T., Begun, D.R., 2019. A new Miocene ape and locomotion in the ancestor of great apes and humans. Nature 575, 489–493.

Bône, A., Louis, M., Martin, B., Durrleman, S., 2018. Deformetrica 4: An open-source software for statistical shape analysis. In: Reuter, M., Wachinger, C., Lombaert, H., Paniagua, B., Lüthi, M., Egger, B. (Eds.), Shape in Medical Imaging, International Workshop, ShapeMI 2018 Held in Conjunction with MICCAI 2018 Granada, Spain, September 20, 2018 Proceedings. LCNS Springer, Cham, pp. 3–13.

Braga, J., Zimmer, V., Dumoncel, J., Samir, C., de Beer, F., Zanolli, C., Pinto, D., Rohlf, F.J., Grine, F.E., 2019. Efficacy of diffeomorphic surface matching and 3D geometric morphometrics for taxonomic discrimination of Early Pleistocene hominin mandibular molars. J. Hum. Evol. 130, 21–35.

Cardini, A., Polly, P.D., 2020. Cross-validated between group PCA scatterplots: A solution to spurious group separation? Evol. Biol. 47, 85–95.

Casanovas-Vilar, I., Alba, D.M., Garcés, M., Robles, J.M., Moyà-Solà, S., 2011. Updated chronology for the Miocene hominoid radiation in Western Eurasia. Proc. Natl. Acad. Sci. USA 108, 5554–5559.

Casanovas-Vilar, I., Alba, D.M., Moyà-Solà, S., Galindo, J., Cabrera, L., Garcés, M., Furió, M., Robles, J.M., Köhler, M., Angelone, C., 2008. Biochronological, taphonomical and paleoenvironmental background of the fossil great ape *Pierolapithecus catalaunicus* (Primates, Hominidae). J. Hum. Evol. 55, 589–603.

Casanovas-Vilar, I., Madern, A., Alba, D.M., Cabrera, L., García-Paredes, I., Van den Hoek Ostende, L.W., DeMiguel, D., Robles, J.M., Furió, M., Van Dam, J., Garcés, M., Angelone, C., Moyà-Solà, S., 2016a. The Miocene mammal record of the Vallès-Penedès Basin (Catalonia). C. R. Palevol 15, 791–812.

Casanovas-Vilar, I., Garcés, M., Van Dam, J., García-Paredes, I., Robles, J.M., Alba, D.M., 2016b. An updated biostratigraphy for the late Aragonian and the Vallesian of the Vallès-Penedès Basin (Catalonia). Geol. Acta 14, 195–217.

Dray, S., Dufour, A., 2007. The ade4 package: Implementing the duality diagram for ecologists. J. Stat. Software 22, 1–20

Dumoncel, J., 2021. RToolsForDeformetrica. R package version 0.1. https://gitlab.com/jeandumoncel/tools-for-deformetrica/-/tree/master/src/R_script/RToolsForDeformetrica.

Durrleman, S., Pennec, X., Trouvé, A., Ayache, N., Braga, J., 2012. Comparison of the endocranial ontogenies between chimpanzees and bonobos via temporal regression and spatiotemporal registration. J. Hum. Evol. 62, 74–88.

Durrleman, S., Prastawa, M., Charon, N., Korenberg, J.R., Joshi, S., Gerig, G., Trouvé, A., 2014. Morphometry of anatomical shape complexes with dense deformations and sparse parameters. Neuroimage 101, 35–49.

Fleagle, J.G., 2013. Primate Adaptation and Evolution, 3rd Ed. Academic Press, San Diego.

Fornai, C., Bookstein, F.L., Weber, G.W., 2015. Variability of *Australopithecus* second maxillary molars from Sterkfontein Member 4. J. Hum. Evol. 85, 181–192.

Fortuny, J., Zanolli, C., Bernardini, F., Tuniz, C., Alba, D.M., 2021. Dryopithecine palaeobiodiversity in the Iberian Miocene revisited on the basis of molar endostructural morphology. Palaeontology 64, 531–554.

Glaunès, J., Joshi, S., 2006. Template estimation from unlabeled point set data and surfaces for computational anatomy. In: Pennec, X., Joshi, S. (Eds.), Proceedings of the International Workshop on the Mathematical Foundations of Computational Anatomy. LNCS Springer, Copenhagen, pp. 29–39.

Harrison, T., 1991. Some observations on the Miocene hominoids from Spain. J. Hum. Evol. 19, 515–520.

Hastie, T., Tibshirani, R., Friedman, J., 2009. The Elements of Statistical Learning, 2nd ed. Springer, New York.

ICZN (International Commission on Zoological Nomenclature), 1999. International Code of Zoological Nomenclature. The International Trust for Zoological Nomenclature, London. https://www.iczn.org/the-code/the-international-codeof-zoological-nomenclature/the-code-online/.

Korenhof, C.A.W., 1961. The enamel-dentine border: a new morphological factor in the study of the (human) molar pattern. Proc. Koninklijke Nederlands 64B, 639–664.

McBrearty, S., Jablonski, N.G., 2005. First fossil chimpanzee. Nature 437, 105–108.

Macchiarelli, R., Bayle, P., Bondioli, L., Mazurier, A., Zanolli, C., 2013. From outer to inner structural morphology in dental anthropology. The integration of the third dimension in the visualization and quantitative analysis of fossil remains. In: Scott, R.G., Irish, J.D. (Eds.), Anthropological Perspectives on Tooth Morphology: Genetics, Evolution, Variation. Cambridge University Press, Cambridge, pp. 250–277.

Marigó, J., Susanna, I., Minwer-Barakat, R., Madurell-Malapeira, J., Moyà-Solà, S., Casanovas-Vilar, I., Robles, J.M., Alba, D.M., 2014. The primate fossil record in the Iberian Peninsula. J. Iber. Geol. 40, 179–211.

Marmi, J., Casanovas-Vilar, I., Robles, J.M., Moyà-Solà, S., Alba, D.M., 2012. The paleoenvironment of *Hispanopithecus laietanus* as revealed by paleobotanical evidence from the Late Miocene of Can Llobateres 1 (Catalonia, Spain). J. Hum. Evol. 62, 412–423.

Martinez Arbizu, P., 2020. pairwiseAdonis: Pairwise multilevel comparison using Adonis. R package version 0.4. https://github.com/pmartinezarbizu/pairwiseAdonis.

Moyà-Solà, S., Köhler, M., 1995. New partial cranium of *Dryopithecus* Lartet, 1863 (Hominoidea, Primates) from the upper Miocene of Can Llobateres, Barcelona, Spain. J. Hum. Evol. 29, 101-139.

Moyà-Solà, S., Köhler, M., Alba, D.M., 2001. *Egarapithecus narcisoi*, a new genus of Pliopithecidae (Primates, Catarrhini) From the Late Miocene of Spain. Am. J. Phys. Anthropol. 114, 312–324.

Moyà-Solà, S., Köhler, M., Alba, D.M., Casanovas-Vilar, I., Galindo, J., 2004. *Pierolapithecus catalaunicus*, a new Middle Miocene great ape from Spain. Science 306, 1339–1344.

Moyà-Solà, S., Köhler, M., Alba, D.M., Casanovas-Vilar, I., Galindo, J., Robles, J.M., Cabrera, L., Garcés, M., Almécija, S., Beamud, E., 2009a. First partial face and upper dentition of the Middle Miocene hominoid *Dryopithecus fontani* from Abocador de Can Mata (Vallès-Penedès

Basin, Catalonia, NE Spain): taxonomic and phylogenetic implications. Am. J. Phys. Anthropol. 139, 126–145.

Moyà-Solà, S., Alba, D.M., Almécija, S., Casanovas-Vilar, I., Köhler, M., De Esteban-Trivigno, S., Robles, J.M., Galindo, J., Fortuny, J., 2009b. A unique Middle Miocene European hominoid and the origins of the great ape and human clade. Proc. Natl. Acad. Sci. USA 106, 9601–9606.

Oksanen, J., Blanchet, F.G., Friendly, M., Kindt, R., Legendre, P., McGlinn, D., Minchin, P.R., O'Hara, R.B., Simpson, G.L., Solymos, P., Stevens, M.H.H., Szoecs, E., Wagner, H., 2020. vegan: Community ecology package. R package version 2.5-7. https://cran.r-project.org/web/packages/vegan/index.html.

Olejniczak, A.J., Martin, L.B., Ulhaas, L., 2004. Quantification of dentine shape in anthropoid primates. Ann. Anat. 186, 479–485.

Pan, L., Dumoncel, J., Mazurier, A., Zanolli, C., 2020. Hominin diversity in East Asia during the Middle Pleistocene: A premolar endostructural perspective. J. Hum. Evol. 148, 102888.

Pan, L., Dumoncel, J., de Beer, F., Hoffman, J., Thackeray, J.F., Duployer, B., Tenailleau, C., Braga, J., 2016. Further morphological evidence on South African earliest *Homo* lower postcanine dentition: enamel thickness and enamel-dentine junction. J. Hum. Evol. 96, 82–96.

Pérez de los Ríos, M., Moyà-Solà, S., Alba, D.M., 2012. The nasal and paranasal architecture of the Middle Miocene ape *Pierolapithecus catalaunicus* (Primates: Hominidae): Phylogenetic implications. J. Hum. Evol. 63, 497–506.

Pérez de los Ríos, M., Alba, D.M., Moyà-Solà, S., 2013. Taxonomic attribution of the La Grive hominoid teeth. Am. J. Phys. Anthropol. 151, 558–565.

Pina, M., Alba, D. M., Almécija, S., Fortuny, J., Moyà-Solà, S., 2012. Brief Communication: Paleobiological inferences on the locomotor repertoire of extinct hominoids based on femoral

neck cortical thickness: the fossil great ape *Hispanopithecus laietanus* as a test-case study. American Journal of Physical Anthropology 149, 142–148.

Pina, M., Alba, D. M., Moyà-Solà, S., Almécija, S., 2019. Femoral neck cortical bone distribution of dryopithecin apes and the evolution of hominid locomotion. Journal of Human Evolution 136, 102651.

Prüfer, K., Munch, K., Hellmann, I., Akagi, K., Miller, J.R., Walenz, B., Koren, S., Sutton, G., Kodira, C., Winer, R., Knight, J.R., Mullikin, J.C., Meader, S.J., Ponting, C.P., Lunter, G., Higashino, S., Hobolth, A., Dutheil, J., Karakoc, E., Alkan, C., Sajjadian, S., Catacchio, C.R., Ventura, M., Marques-Bonet, T., Eichler, E.E., André, C., Atencia, R., Mugisha, L., Junhold, J., Patterson, N., Siebauer, M., Good, J.M., Fischer, A., Ptak, S.E., Lachmann, M., Symer, D.E., Mailund, T., Schierup, M.H., Andrés, A.M., Kelso, J., Pääbo, S., 2012. The bonobo genome compared with the chimpanzee and human genomes. Nature 486, 527–531.

Pugh, K.D., 2022. Phylogenetic analysis of Middle-Late Miocene apes. J. Hum. Evol. 165, 103140.

R Core Team, 2022. R: A language and environment for statistical computing. R Foundation for Statistical Computing, Vienna.

Schlager, S., 2020. Morpho: calculations and visualizations related to geometric morphometrics. R package version 2.8. http://cran.r-project.org/web/packages/Morpho/index.html.

Skinner, M.M., Wood, B.A., Boesch, C., Olejniczak, A.J., Rosas, A., Smith, T., Hublin, J.-J., 2008. Dental trait expression at the enamel-dentine junction of lower molars in extant and fossil hominoids. J. Hum. Evol. 54, 173–186.

Skinner, M.M., Gunz, P., Wood, B.A., Boesch, C., Hublin, J.-J., 2009. Discrimination of extant *Pan* species and subspecies using the enamel-dentine junction morphology of lower molars. Am. J. Phys. Anthropol. 140, 234–243.

Spoor, F., Gunz, P., Neubauer, S., Stelzer, S., Scott, N., Kwekason, A., Dean, M.C., 2015. Reconstructed *Homo habilis* type OH 7 suggests deep-rooted species diversity in early *Homo*. Nature 519, 83–86.

Urciuoli, A., Zanolli, C., Beaudet, A., Dumoncel, J., Santos, F., Moyà-Solà, S., Alba, D.M., 2020. The evolution of the vestibular apparatus in apes and humans. eLife 9, e51261.

Urciuoli, A., Zanolli, C., Almécija, S., Beaudet, A., Dumoncel, J., Morimoto, N., Nakatsukasa, M., Moyà-Solà, S., Begun, D.R., Alba, D.M., 2021b. Reassessment of the phylogenetic relationships of the late Miocene apes *Hispanopithecus* and *Rudapithecus* based on vestibular morphology. Proc. Natl. Acad. Sci. USA 118, e2015215118.

Urciuoli, A., Zanolli, C., Beaudet, A., Pina, M., Almécija, S., Moyà-Solà, S., Alba, D.M., 2021a. A comparative analysis of the vestibular apparatus in *Epipliopithecus vindobonensis*: Phylogenetic implications. J. Hum. Evol. 151, 102930.

Zanolli, C., Grine, F.E., Kullmer, O., Schrenk, F., Macchiarelli, R., 2015. Brief Communication: The Early Pleistocene deciduous hominid molar FS-72 from the Sangiran Dome of Java, Indonesia: A taxonomic reappraisal based on its comparative endostructural characterization. Am. J. Phys. Anthropol. 157, 666–674.

Zanolli, C., Bayle, P., Bondioli, L., Dean, M.C., Le Luyer, M., Mazurier, A., Morita, W., Macchiarelli, R., 2017. Is the deciduous/permanent molar enamel thickness ratio a taxon-specific indicator in extant and extinct hominids? C.R. Palevol. 16, 702–714.

Zanolli, C., Pan, L., Dumoncel, J., Kullmer, O., Kundrat, M., Liu, W., Macchiarelli, R., Mancini, L., Schrenk, F., Tuniz, C., 2018. Inner tooth morphology of *Homo erectus* from Zhoukoudian. New evidence from an old collection housed at Uppsala University, Sweden. J. Hum. Evol. 116, 1–13.

Zanolli, C., Kullmer, O., Kelley, J., Bacon, A.M., Demeter, F., Dumoncel, J., Fiorenza, L., Grine, F.E., Hublin, J.J., Anh Tuan, N., Thi Mai Huong, N., Pan, L., Schillinger, B., Schrenk, F., Skinner, M.M., Ji, X., Macchiarelli, R., 2019. Evidence for increased hominid diversity in the Early-Middle Pleistocene of Indonesia. Nat. Ecol. Evol. 3, 755–764.

Zanolli, C., Kaifu, Y., Pan, L., Xing, S., Mijares, A.S., Kullmer, O., Schrenk, F., Corny, J., Dizon, E., Robles, E., Détroit, F., 2022a. Further analyses of the structural organization of *Homo luzonensis* teeth: Evolutionary implications. J. Hum. Evol. 163, 103124.

Zanolli, C., Urciuoli, A., Delgado, M., Davies, T.W., Bouchet, F., Fortuny, J., Beaudet, A., Alba, D.M., Kullmer, O., Skinner M.M., 2022 The phylogenetic signal of the enamel-dentine junction of primate molars. Am. J. Phys. Anthropol. 177, 202.

Figure captions

Figure 1. Main nonmetric features distinguishing between the Miocene dryopithecine genera at the enamel-dentine junction (EDJ) level of the maxillary (A) and mandibular (B) molars. The EDJ of molars of *Pierolapithecus catalaunicus* (M^2 IPS21350), *Dryopithecus fontani* (M^2: IPS35026 and M_2 2004.HARLE.46), *Anoiapithecus brevirostris* (M^2 and M^1 IPS43000), '*Sivapithecus*' *occidentalis* (IPS 1826), *Hispanopithecus crusafonti* (M^2 IPS1820 and M_1 IPS1816), and *Hispanopithecus laietanus* (M^2 IPS18000.5 and M_2 IPS 1804) are illustrated in occlusal and buccal views. Symbols: black arrow = buccolingual constriction (waisting); plus = deep and well-delineated mesial fovea; cross = small lingual cingulum-like trait; asterisk = peripherally-placed protocone dentine horn; circle = internally-tilted metaconid dentine horn; minus = pit-like cingulum; white arrow = lingual accessory dentine horn.

Figure 2. Bivariate plot of the between-group principal component 2 (bgPC2) against the between-group component 1 (bgPC1) based on the diffeomorphic surface matching analyses of the enamel-dentine junction of the M^1 (A), M^2 (B), M^3 (C), M_1 (D), M_2 (E), and M_3 (F) of the Miocene dryopithecine genera compared with the extant great apes. Percentage of variance for each axis is provided within parentheses in the figure. The surfaces at the end of the axes illustrate the extreme shapes along each component.

Figure 3. Bivariate plot of the between-group principal component 2 (bgPC2) against the between-group component 1 (bgPC1) based on the diffeomorphic surface matching analyses of the enamel-dentine junction of the M_1 (A), M_2 (B), M_3 (C) , M_1 (D), M_2 (E), and M_3 (F) of the Miocene dryopithecine genera compared with the extant great apes. Percentage of variance for each axis is provided within parentheses in the figure. The surfaces at the end of the axes illustrate the extreme shapes along each component.

Figure 4. Plots of the Euclidian distances between specimens of the Miocene dryopithecines (upper part of each panel) and between extant great apes based on the between-group principal components computed for the M^1 (A), M^2 (B), M^3 (C), M_1 (D), M_2 (E), and M_3 (F). For both intra- and intergeneric variations, minimum (5%) and maximum (95%) limits are represented by vertical dotted lines. Abbreviations: A = *Anoiapithecus*; H = *Hispanopithecus*; D = *Dryopithecus*; P = *Pierolapithecus*; S = '*Sivapithecus*' *occidentalis*; A-D = distance between *Anoiapithecus* and *Dryopithecus* specimens; A-P = distance between *Anoiapithecus* and *Pierolapithecus* specimens; H-D = distance between *Hispanopithecus* and *Dryopithecus* specimens; H-P = distance between *Hispanopithecus* and *Pierolapithecus* specimens; H-A = distance between *Hispanopithecus* and *Anoiapithecus* specimens; H-S = distance between *Hispanopithecus* and '*Sivapithecus*'

occidentalis specimens; P-D = distance between *Pierolapithecus* and *Dryopithecus* specimens; D-S = distance between *Dryopithecus* and '*Sivapithecus*' *occidentalis* specimens.

Figure 5. Plots of the Euclidian distances between specimens of the Miocene dryopithecines (upper part of each panel) and between extant great apes based on the canonical variates computed for the M^1 (A), M^2 (B), M^3 (C), M_1 (D), M_2 (E), and M_3 (F). For both intra- and inter-generic variations, minimum (5%) and maximum (95%) limits are represented by vertical dotted lines. Abbreviations: A = *Anoiapithecus*; H = *Hispanopithecus*; D = *Dryopithecus*; P = *Pierolapithecus*; S = '*Sivapithecus*' *occidentalis*; A-D = distance between *Anoiapithecus* and *Dryopithecus* specimens; A-P = distance between *Anoiapithecus* and *Pierolapithecus* specimens; H-D = distance between *Hispanopithecus* and *Dryopithecus* specimens; H-P = distance between *Hispanopithecus* and *Pierolapithecus* specimens; H-A = distance between *Hispanopithecus* and *Anoiapithecus* specimens; H-S = distance between *Hispanopithecus* and '*Sivapithecus*' *occidentalis* specimens; P-D = distance between *Pierolapithecus* and *Dryopithecus* specimens; D-S = distance between *Dryopithecus* and '*Sivapithecus*' *occidentalis* specimens.

Table 1

Typicality probabilities of the investigated dryopithecine specimens with respect to the extant great apes based on the between–group principal component analysis (bgPCA) and canonical variate analysis (CVA).[a]

Miocene genus	Catalog No.	Tooth	*p* (bgPCA)			*p* (CVA)		
			Gorilla	*Pan*	*Pongo*	*Gorilla*	*Pan*	*Pongo*
A	IPS35027	M^1 L	<0.01	<0.01	<0.01	<0.01	<0.01	**0.05**
A	IPS35027	M^1 R	<0.01	<0.01	0.02	<0.01	<0.01	**0.08**
A	IPS43000	M^1 L	<0.01	<0.01	<0.01	<0.01	<0.01	**0.18**
A	IPS43000	M^1 R	<0.01	<0.01	<0.01	<0.01	<0.01	**0.48**
D	IPS35026	M^1	<0.01	<0.01	<0.01	<0.01	<0.01	**0.75**
H	IPS1815	M^1	<0.01	<0.01	0.04	<0.01	<0.01	**0.24**
H	IPS1818	M^1	<0.01	<0.01	0.03	<0.01	<0.01	**0.19**
H	IPS1844	M^1	<0.01	<0.01	0.03	<0.01	<0.01	**0.28**
P	IPS21350	M^1	<0.01	<0.01	<0.01	<0.01	<0.01	**0.93**
A	IPS35027	M^2 L	<0.01	<0.01	<0.01	<0.01	<0.01	<0.01
A	IPS35027	M^2 R	<0.01	<0.01	<0.01	<0.01	0.01	<0.01
A	IPS43000	M^2 L	<0.01	<0.01	<0.01	<0.01	**0.06**	<0.01
A	IPS43000	M^2 R	<0.01	<0.01	<0.01	<0.01	**0.09**	<0.01
D	IPS35026	M^2	<0.01	<0.01	<0.01	<0.01	<0.01	**0.07**
D	MGSB48486	M^2	<0.01	<0.01	<0.01	<0.01	<0.01	0.02
H	IPS1820	M^2	<0.01	<0.01	<0.01	<0.01	0.02	0.02

H	IPS1844	M^2	<0.01	<0.01	<0.01	<0.01	**0.08**	<0.01
H	IPS58339	M^2	<0.01	<0.01	**0.10**	<0.01	<0.01	**0.36**
H	IPS180005	M^2	<0.01	<0.01	0.01	<0.01	<0.01	**0.13**
P	IPS21350	M^2 L	<0.01	<0.01	<0.01	<0.01	<0.01	0.02
P	IPS21350	M^2 R	<0.01	<0.01	<0.01	<0.01	<0.01	<0.01
A	IPS43000	M^3	<0.01	<0.01	<0.01	<0.01	<0.01	**0.50**
D	IPS35026	M^3	<0.01	<0.01	**0.53**	<0.01	<0.01	**0.99**
H	IPS1812	M^3	<0.01	<0.01	<0.01	<0.01	<0.01	**0.38**
H	IPS1814	M^3	<0.01	<0.01	<0.01	<0.01	<0.01	**0.42**
H	IPS1772	M^3	<0.01	<0.01	0.01	<0.01	<0.01	**0.06**
H	IPS58340	M^3	<0.01	<0.01	0.03	<0.01	<0.01	**0.32**
H	IPS180005	M^3	<0.01	<0.01	0.02	<0.01	<0.01	**0.27**
P	IPS21350	M^3	<0.01	<0.01	<0.01	<0.01	<0.01	<0.01
A	IPS43000	M_1 L	<0.01	<0.01	<0.01	<0.01	<0.01	0.04
A	IPS43000	M_1 R	<0.01	<0.01	<0.01	<0.01	<0.01	**0.30**
D	HARLE 46	M_1	<0.01	<0.01	<0.01	<0.01	<0.01	**0.19**
H	MGSB25314	M_1	<0.01	<0.01	<0.01	<0.01	<0.01	<0.01
H	IPS1797	M_1	<0.01	<0.01	<0.01	<0.01	<0.01	<0.01
H	IPS1802	M_1	<0.01	<0.01	<0.01	<0.01	<0.01	<0.01
H	IPS1816	M_1	<0.01	<0.01	<0.01	<0.01	<0.01	<0.01
D	HARLE 44	M_2	<0.01	<0.01	<0.01	<0.01	<0.01	0.01
D	HARLE 46	M_2	<0.01	<0.01	<0.01	<0.01	<0.01	**0.25**

H	MGSB25314	M_2	<0.01	<0.01	<0.01	<0.01	<0.01	<0.01
H	IPS1780	M_2	<0.01	<0.01	<0.01	<0.01	<0.01	<0.01
H	IPS1797	M_2	<0.01	<0.01	<0.01	<0.01	<0.01	<0.01
H	IPS1802	M_2	<0.01	<0.01	<0.01	<0.01	<0.01	**0.05**
H	IPS1804	M_2	<0.01	<0.01	<0.01	<0.01	<0.01	<0.01
So	IPS1826	M_2	<0.01	<0.01	<0.01	<0.01	<0.01	**0.13**
So	IPS41734	M_2	<0.01	<0.01	<0.01	<0.01	<0.01	0.03
D	HARLE44	M_3	<0.01	<0.01	<0.01	<0.01	<0.01	**0.41**
D	HARLE47	M_3	<0.01	<0.01	<0.01	<0.01	<0.01	**0.84**
H	MGSB25314	M_3	<0.01	<0.01	<0.01	<0.01	<0.01	**0.61**
H	IPS1802	M_3	<0.01	<0.01	<0.01	<0.01	<0.01	**0.52**
H	IPS1822	M_3	<0.01	<0.01	0.04	<0.01	<0.01	0.03
So	IPS1827	M_3	<0.01	<0.01	<0.01	<0.01	<0.01	**0.26**

Abbreviations: L = left; R = right; A = *Anoiapithecus*; D = *Dryopithecus*; P = *Pierolapithecus*; So = '*Sivapithecus*' *occidentalis* species inquirenda.

[a] These probabilities denote the likelihood that the score of each fossil specimen fits with a particular group, not the likelihood of group membership in each of the a priori defined groups given a particular score. The highest probabilities (above statistical threshold of 0.05) are highlighted in bold for each fossil specimen.

Table 2

Results of permutation tests, given as both probabilities (interpreted as *p*-values) and frequencies (within parentheses), based on the between-group principal component analysis (bgPCA) and canonical variate analysis (CVA) comparing the intrageneric variation of dryopithecine genera with that of extant great apes. [a]

Miocene genus	Tooth	*n*	bgPCA			CVA		
			Gorilla	*Pan*	*Pongo*	*Gorilla*	*Pan*	*Pongo*
A	M^1	4	0.67 (140/210)	0.98 (206/210)	0.99 (208/210)	0.67 (141/210)	0.99 (208/210)	1 (209/210)
H	M^1	3	0.48 (58/120)	0.88 (106/120)	0.93 (112/120)	0.54 (65/120)	0.94 (113/120)	0.97 (116/120)
D	M^2	2	0.47 (21/45)	0.40 (18/45)	0.47 (21/45)	0.96 (43/45)	0.76 (34/45)	0.87 (39/45)
H	M^2	4	0.76 (159/210)	0.71 (148/210)	0.69 (145/210)	0.86 (180/210)	0.50 (105/210)	0.64 (135/210)
P	M^2	2	0.64 (29/45)	0.62 (28/45)	0.62 (28/45)	0.87 (39/45)	0.71 (32/45)	0.80 (36/45)
H	M^3	5	**0 (0/252)**	**0 (0/252)**	0.39 (97/252)	**0 (0/252)**	**0 (0/252)**	0.65 (164/252)
A	M_1	2	0.80 (36/45)	0.80 (36/45)	0.82 (37/45)	0.73 (33/45)	0.73 (33/45)	0.87 (39/45)
H	M_1	3	0.93 (112/120)	0.98 (118/120)	0.98 (117/120)	0.52 (62/120)	0.65 (78/120)	0.84 (101/120)
D	M_2	2	0.22 (10/45)	0.49 (22/45)	0.49 (22/45)	0.38 (17/45)	0.58 (26/45)	0.64 (29/45)
H	M_2	6	**0 (0/210)**	**0.02 (5/210)**	0.33 (69/210)	**0 (0/210)**	**0 (0/210)**	**0 (0/210)**
So	M_2	2	0.93 (42/45)	0.96 (43/45)	0.93 (42/45)	0.82 (37/45)	0.89 (40/45)	0.93 (42/45)
D	M_3	2	0.09 (4/45)	0.11 (5/45)	0.22 (10/45)	0.24 (11/45)	0.53 (24/45)	0.53 (24/45)
H	M_3	3	0.18 (21/120)	0.28 (33/120)	0.45 (54/120)	0.23 (27/120)	0.47 (56/120)	0.43 (51/120)

Abbreviations: A = *Anoiapithecus*; D = *Dryopithecus*; P = *Pierolapithecus*; So = '*Sivapithecus*' *occidentalis* species inquirenda.

[a] Variation in dryopithecines exceeds that seen in extant apes when $p < 0.05$. Probabilities lower than 0.05 are bolded.

Table 3

Results of permutation tests, given as both probabilities (interpreted as *p*-values) and frequencies (within parentheses), based on the between-group principal component analysis (bgPCA) and canonical variate analysis (CVA) comparing the variation of combined dryopithecine samples with the intrageneric variation of extant great apes. [a]

Miocene genera	Tooth	*n*	bgPCA			CVA		
			Gorilla	*Pan*	*Pongo*	*Gorilla*	*Pan*	*Pongo*
A + D + P	M^1	6	**0 (0/210)**	0.31 (65/210)	1 (210/210)	0.33 (70/210)	0.91 (190/210)	0.15 (31/210)
A + D	M^1	5	0.48 (12/252)	0.80 (201/252)	1 (252/252)	0.68 (172/252)	0.96 (243/252)	1 (252/252)
A + P	M^1	5	**0 (0/252)**	0.47 (118/252)	0.99 (250/252)	0.14 (36/252)	0.82 (206/252)	1 (252/252)
D + P	M^1	2	0.78 (35/45)	0.89 (40/45)	0.91 (41/45)	0.67 (30/45)	0.89 (40/45)	0.91 (41/45)
A + D + P	M^2	8	**0 (0/45)**	**0 (0/45)**	**0 (0/45)**	**0 (0/45)**	**0 (0/45)**	**0 (0/45)**
A + D	M^2	6	**0 (0/210)**	**0 (0/210)**	**0 (0/210)**	**0 (0/210)**	**0 (0/210)**	**0 (0/210)**
A + P	M^2	6	0.98 (205/210)	0.90 (1895/210)	0.90 (188/210)	0.98 (205/210)	0.61 (141/210)	0.75 (158/210)
D + P	M^2	4	**0 (0/210)**	0.20 (41/210)	**0.03 (6/210)**	0.22 (46/210)	0.23 (48/210)	0.11 (23/210)
A + D + P	M^3	3	**0 (0/120)**	**0 (0/120)**	0.19 (23/120)	**0 (0/120)**	**0 (0/120)**	0.25 (30/120)
A + D	M^3	2	0.27 (12/45)	**0.04 (2/45)**	0.67 (30/45)	0.56 (25/45)	0.51 (23/45)	0.78 (35/45)
A + P	M^3	2	**0 (0/45)**	**0 (0/45)**	0.42 (19/45)	**0 (0/45)**	**0 (0/45)**	**0 (0/45)**
D + P	M^3	2	**0 (0/45)**	**0 (0/45)**	**0 (0/45)**	**0 (0/45)**	**0 (0/45)**	**0 (0/45)**
A + D	M_1	3	0.98 (117/120)	0.98 (118/120)	0.98 (118/120)	0.66 (79/20)	0.75 (90/120)	0.88 (105/120)
D + So	M_2	4	0.76 (160/210)	0.92 (193/210)	0.83 (175/210)	0.74 (155/210)	0.95 (199/210)	0.98 (206/210)
D + So	M_3	3	0.22 (26/120)	0.46 (55/120)	0.52 (62/120)	0.33 (40/120)	0.71 (85/120)	0.79 (95/120)

Abbreviations: A = *Anoiapithecus*; D = *Dryopithecus*; P = *Pierolapithecus*; So = '*Sivapithecus*' *occidentalis* species inquirenda.

[a] Variation in dryopithecines exceeds that seen in extant apes when $p < 0.05$. Probabilities lower than 0.05 are bolded.

A

Pierolapithecus catalaunicus

Dryopithecus fontani

Anoiapithecus brevirostris

Hispanopithecus crusafonti

Hispanopithecus laietanus

occ

5 mm

bucc

B

'*Sivapithecus*' *occidentalis*

Dryopithecus fontani

Anoiapithecus brevirostris

Hispanopithecus crusafonti

Hispanopithecus laietanus

occ

bucc

A

M¹

IPS43000
IPS35026
IPS21350
IPS1844
IPS1818
IPS1815
IPS35027
Pongo
Gorilla
Pan

bgPC2 (35.70 %)
bgPC1 (64.30 %)

Anoiapithecus
Dryopithecus
Hispanopithecus
Pierolapithecus

B

M²

IPS58339
IPS1820
IPS18000.5
MGSB48486
IPS1844
IPS35026
IPS21350
IPS43000
IPS35027
Pongo
Gorilla
Pan

bgPC2 (31.64 %)
bgPC1 (68.36 %)

Anoiapithecus
Dryopithecus
Hispanopithecus
Pierolapithecus

C

M³

IPS58340
IPS1772
IPS35026
IPS18000.5
IPS43000
IPS1814
IPS1812
IPS21350
Pongo
Gorilla
Pan

bgPC2 (29.07 %)
bgPC1 (70.93 %)

Anoiapithecus
Dryopithecus
Hispanopithecus
Pierolapithecus

D

M$_1$

2004.HARLE.46
IPS43000
MGSB25314
IPS1802
IPS1816
IPS1797
Pongo
Gorilla
Pan

bgPC2 (33.26 %)
bgPC1 (66.74 %)

Anoiapithecus
Dryopithecus
Hispanopithecus

E

M$_2$

2004.HARLE.44
2004.HARLE.46
MGSB25314
IPS1826
IPS41734
IPS1804
IPS1802
IPS1797
IPS1780
Pongo
Gorilla
Pan

bgPC2 (24.35 %)
bgPC1 (75.65 %)

Dryopithecus
Hispanopithecus
'S.' occidentalis

F

M$_3$

2004.HARLE.47
2004.HARLE.44
IPS1822
IPS1827
MGSB25314
IPS1802
Pongo
Gorilla
Pan

bgPC2 (27.99 %)
bgPC1 (72.01 %)

Dryopithecus
Hispanopithecus
'S.' occidentalis

A

M¹

IPS35027
IPS43000
IPS1815
IPS1818
IPS1844
IPS21350
IPS35026
Pan
Gorilla
Pongo
Anoiapithecus
Dryopithecus
Hispanopithecus
Pierolapithecus
CV2 (23.24 %)
CV1 (76.76 %)

D

M$_1$

IPS1797
IPS1802
IPS43000
MGSB25314
IPS1816
2004.HARLE.46
Pongo
Gorilla
Pan
Anoiapithecus
Dryopithecus
Hispanopithecus
CV2 (23.26 %)
CV1 (76.74 %)

B

M²

IPS35027
IPS21350
IPS1820
IPS43000
IPS1844
IPS35026
MGSB48486
IPS58339
IPS18000.5
Pan
Pongo
Gorilla
Anoiapithecus
Dryopithecus
Hispanopithecus
Pierolapithecus
CV2 (20.54 %)
CV1 (79.46 %)

E

M$_2$

IPS1780
MGSB25314
IPS1802
IPS41734
IPS1797
IPS1804
2004.HARLE.44
IPS1826
2004.HARLE.46
Pongo
Gorilla
Pan
Dryopithecus
Hispanopithecus
'S.' occidentalis
CV2 (5.70 %)
CV1 (94.30 %)

C

M³

Pan
Gorilla
IPS35026
Pongo
IPS1812
IPS1814
IPS18000.5
IPS43000
IPS1772
IPS58340
IPS21350
Anoiapithecus
Dryopithecus
Hispanopithecus
Pierolapithecus
CV2 (27.84 %)
CV1 (72.16 %)

F

M$_3$

IPS1827
2004.HARLE.44
2004.HARLE.47
MGSB25314
IPS1802
Gorilla
Pongo
Pan
IPS1822
Dryopithecus
Hispanopithecus
'S.' occidentalis
CV2 (40.32 %)
CV1 (59.68 %)

A

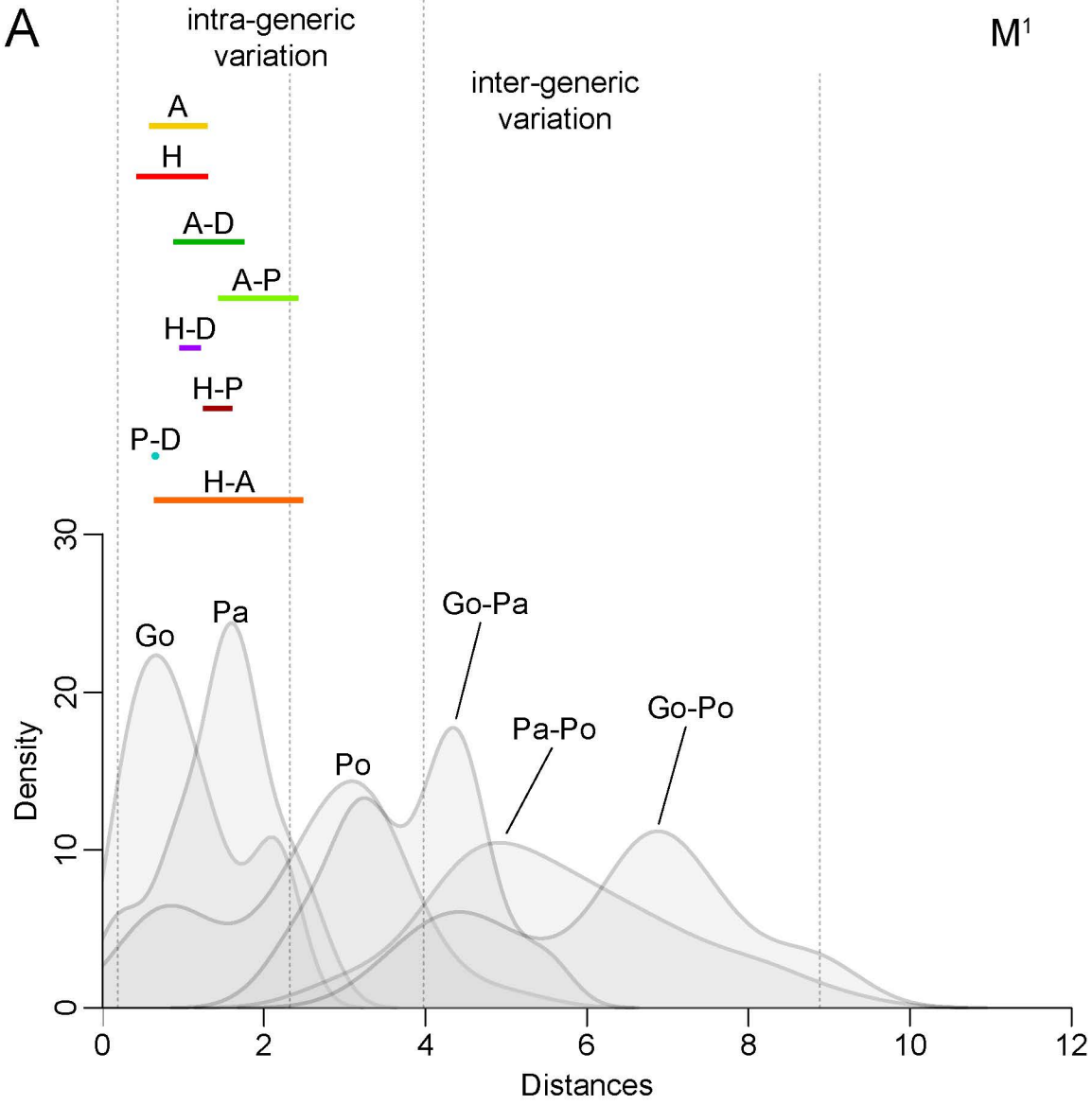
intra-generic variation
inter-generic variation
M1
A
H
A-D
A-P
H-D
H-P
P-D
H-A
Go
Pa
Po
Go-Pa
Pa-Po
Go-Po
Density
0
10
20
30
0
2
4
6
8
10
12
Distances

D

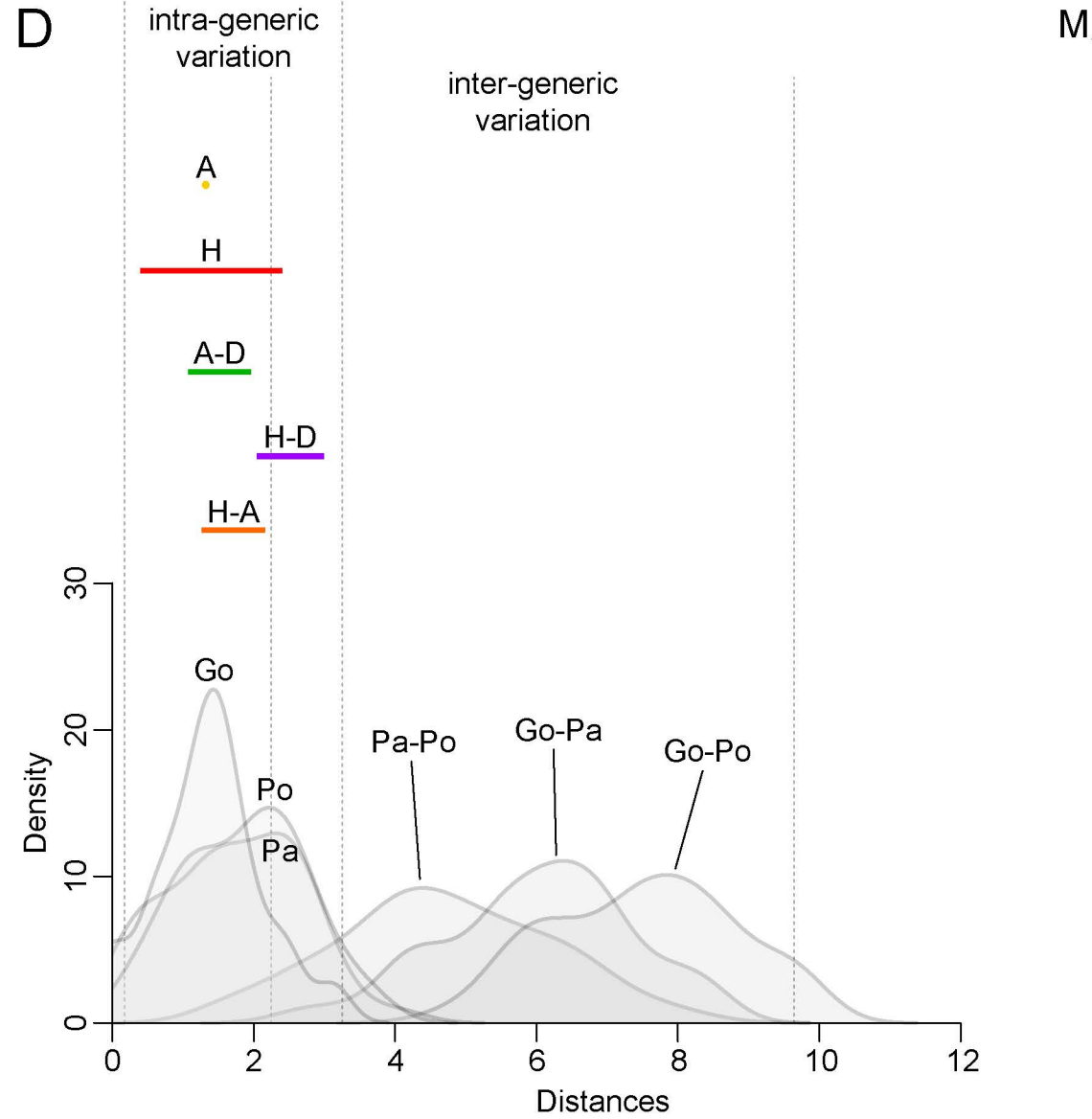
intra-generic variation
inter-generic variation
M1
A
H
A-D
H-D
H-A
Go
Po
Pa
Pa-Po
Go-Pa
Go-Po
Density
0
10
20
30
0
2
4
6
8
10
12
Distances

B

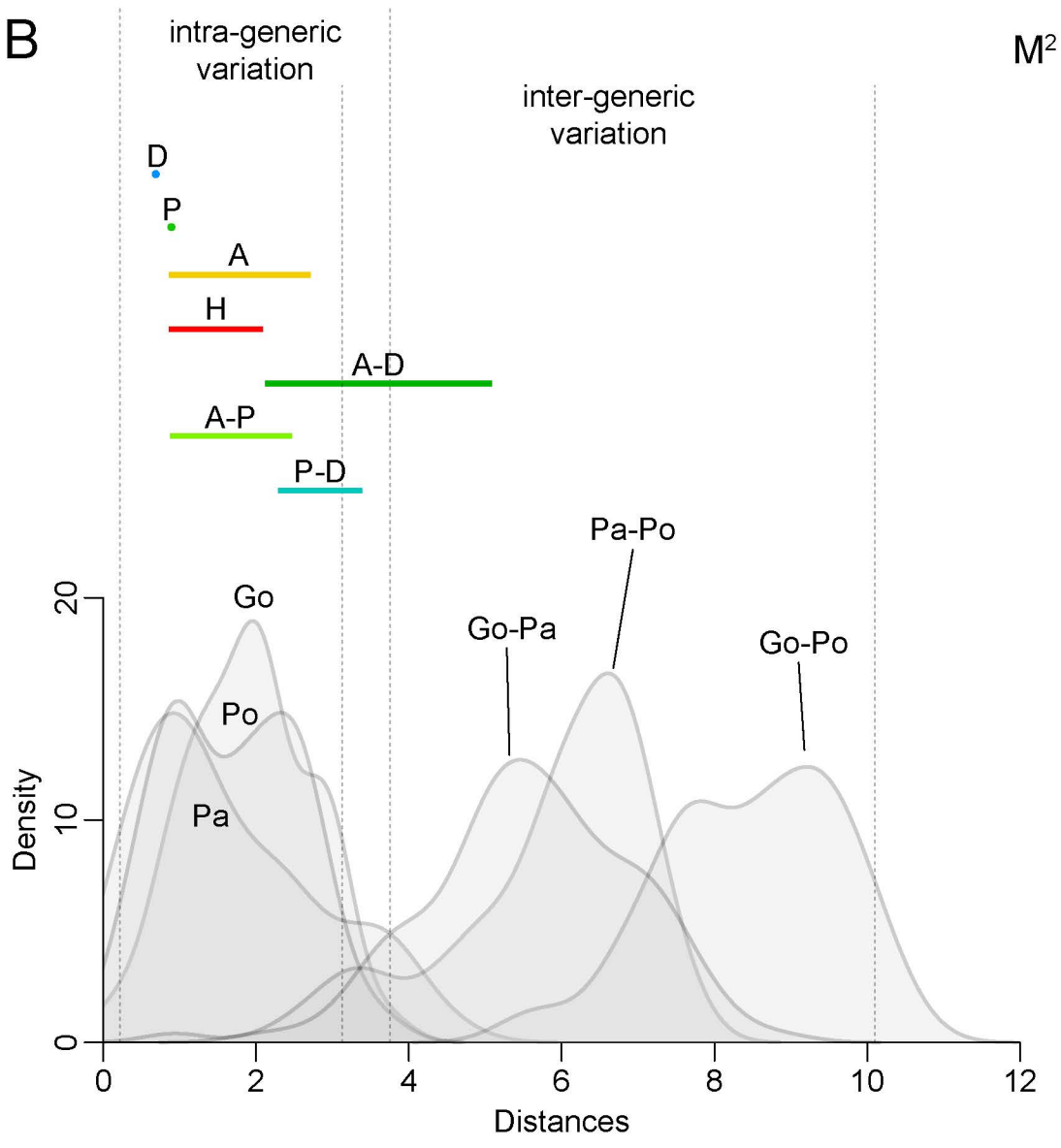
intra-generic variation
inter-generic variation
M2
D
P
A
H
A-D
A-P
P-D
H-A
Go
Po
Pa
Go-Pa
Pa-Po
Go-Po
Density
0
10
20
0
2
4
6
8
10
12
Distances

E

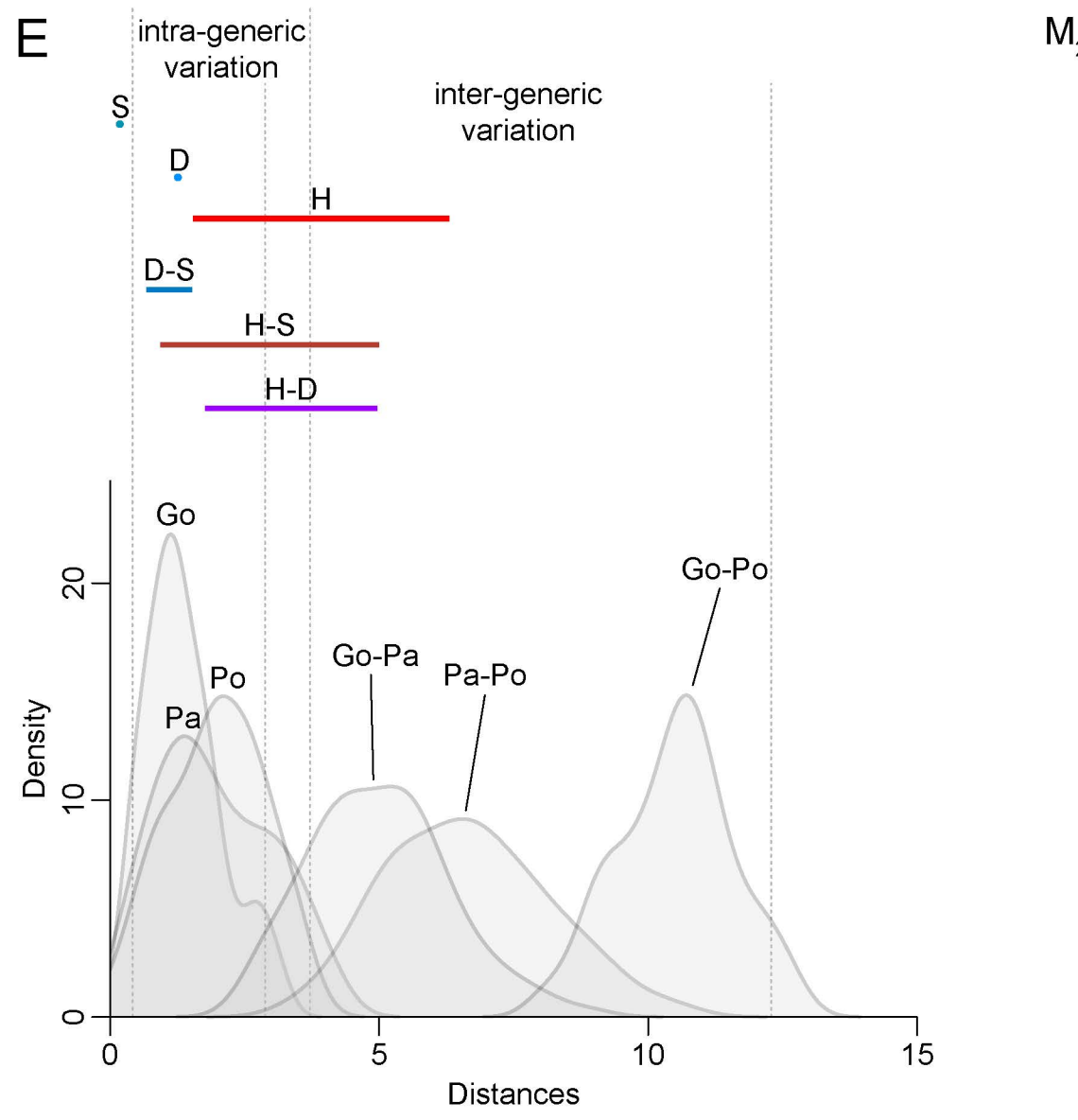
intra-generic variation
inter-generic variation
M2
S
D
H
D-S
H-S
H-D
Go
Po
Pa
Go-Pa
Pa-Po
Go-Po
Density
0
10
20
0
5
10
15
Distances

C

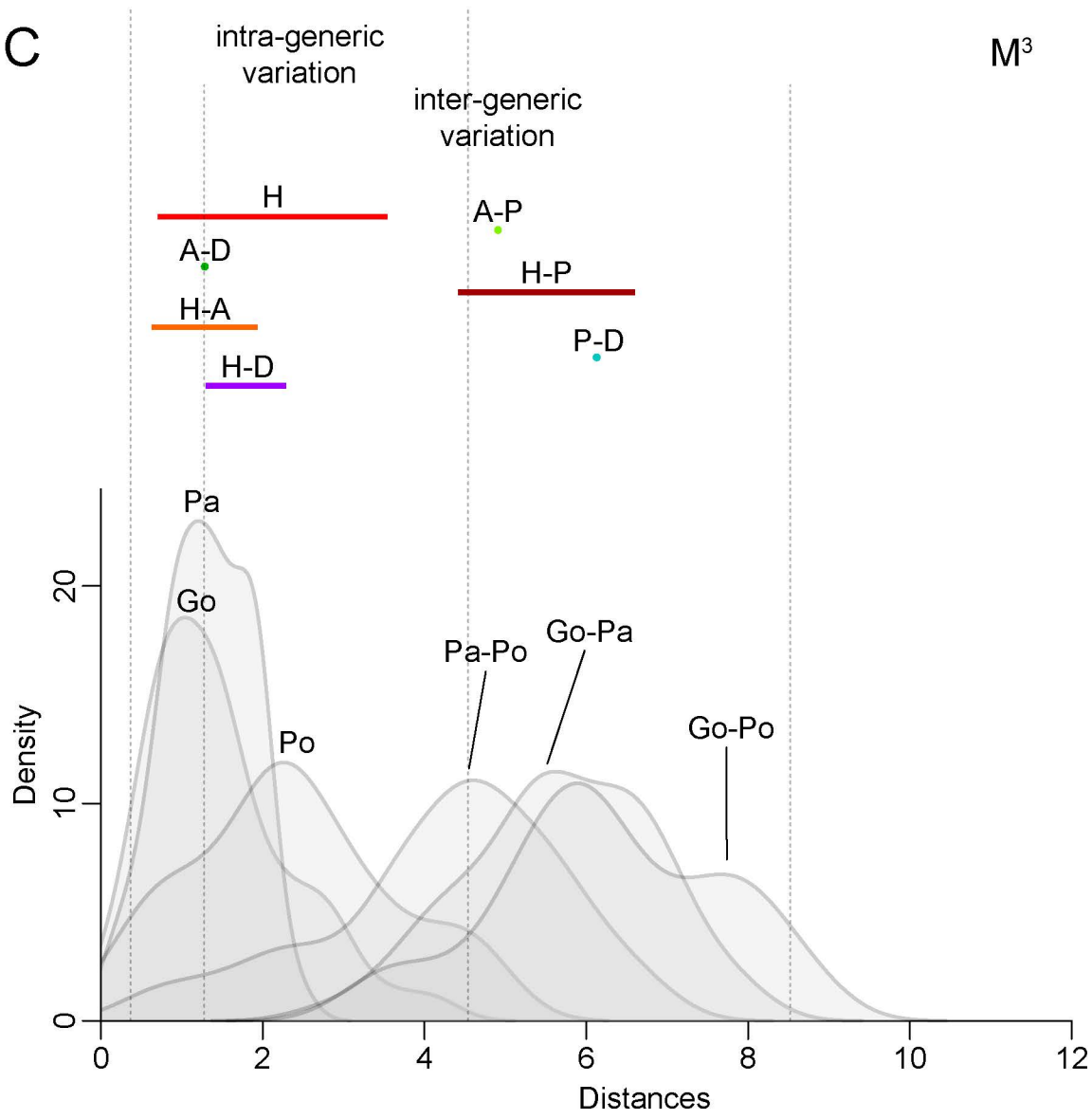
intra-generic variation
inter-generic variation
M3
H
A-D
A-P
H-P
H-A
H-D
P-D
Pa
Go
Po
Pa-Po
Go-Pa
Go-Po
Density
0
10
20
0
2
4
6
8
10
12
Distances

F

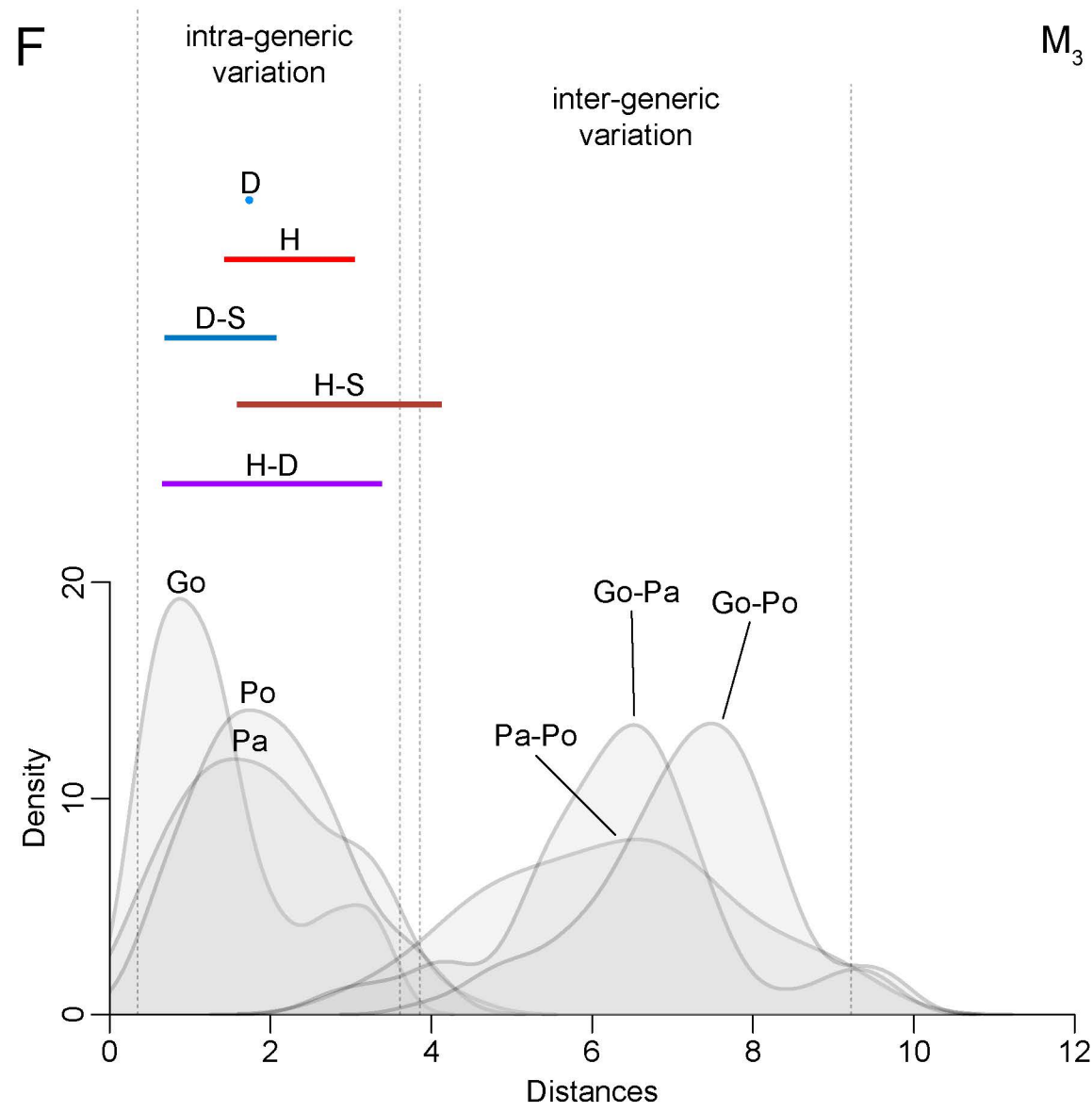
intra-generic variation
inter-generic variation
M3
D
H
D-S
H-S
H-D
Go
Po
Pa
Pa-Po
Go-Pa
Go-Po
Density
0
10
20
0
2
4
6
8
10
12
Distances

A

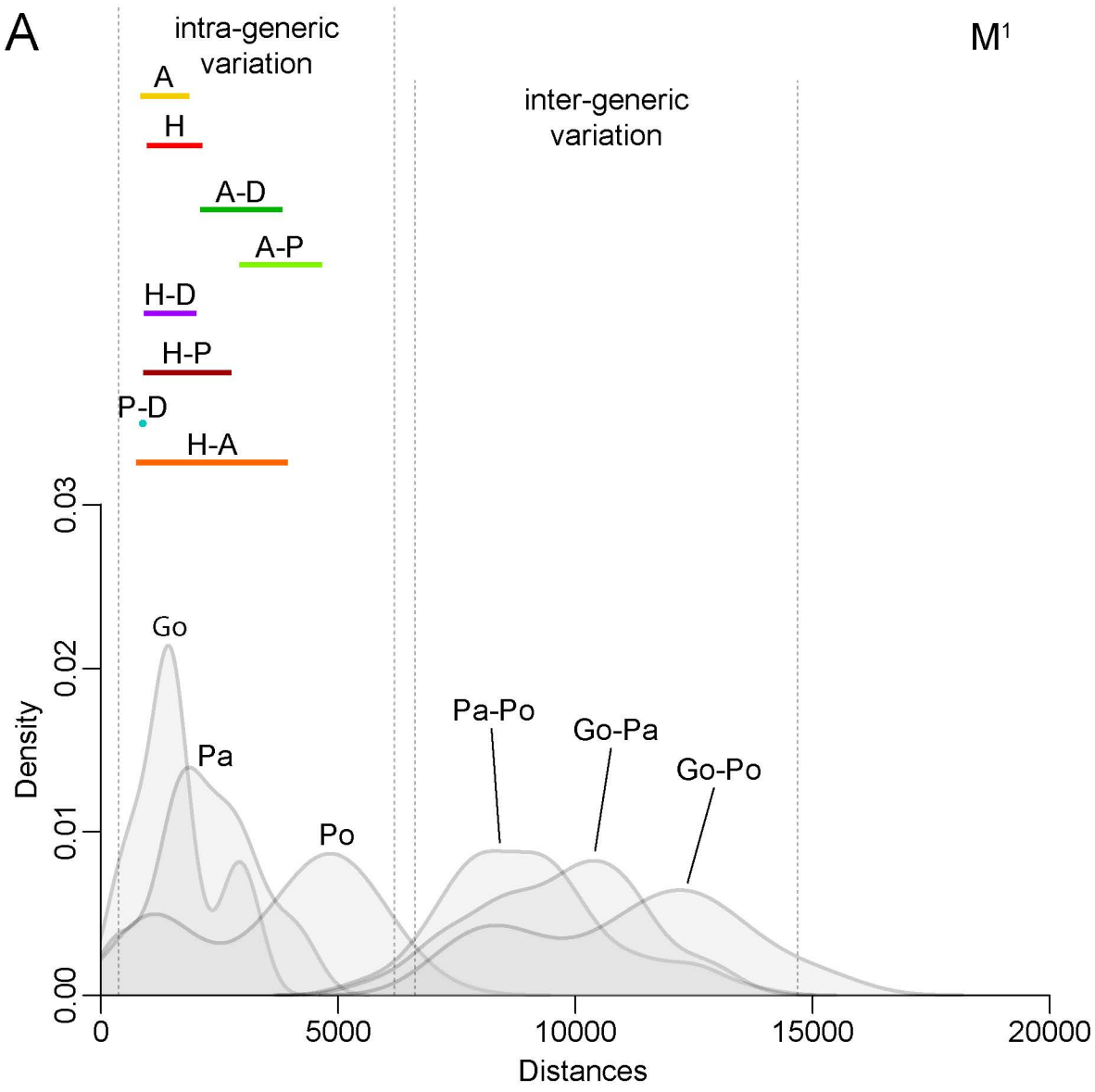
intra-generic variation
inter-generic variation
M1
A
H
A-D
A-P
H-D
H-P
P-D
H-A
Go
Pa
Po
Pa-Po
Go-Pa
Go-Po
Density
0.00
0.01
0.02
0.03
0
5000
10000
15000
20000
Distances

D

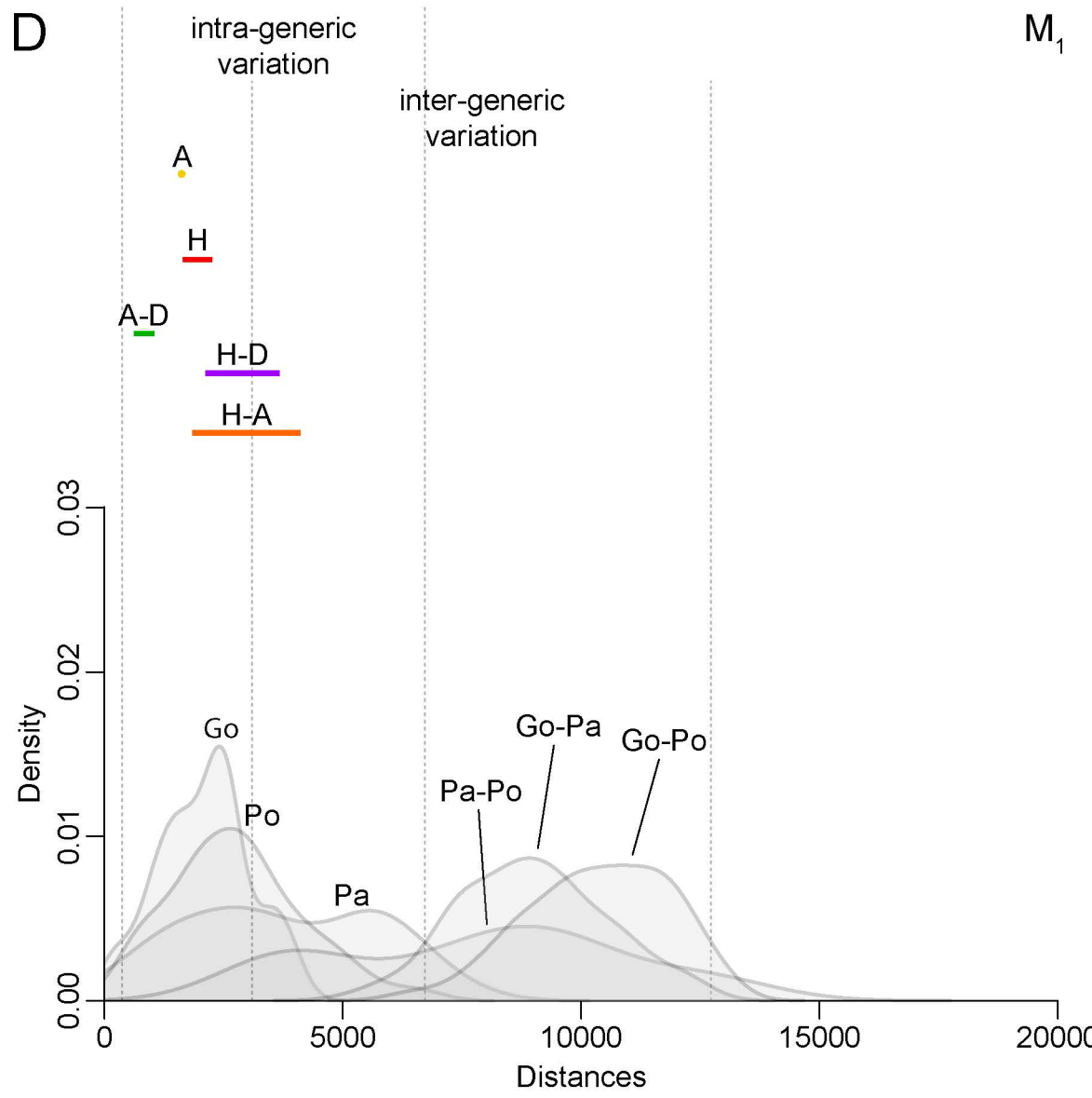
intra-generic variation
inter-generic variation
M1
A
H
A-D
H-D
H-A
Go
Po
Pa
Pa-Po
Go-Pa
Go-Po
Density
0.00
0.01
0.02
0.03
0
5000
10000
15000
20000
Distances

B

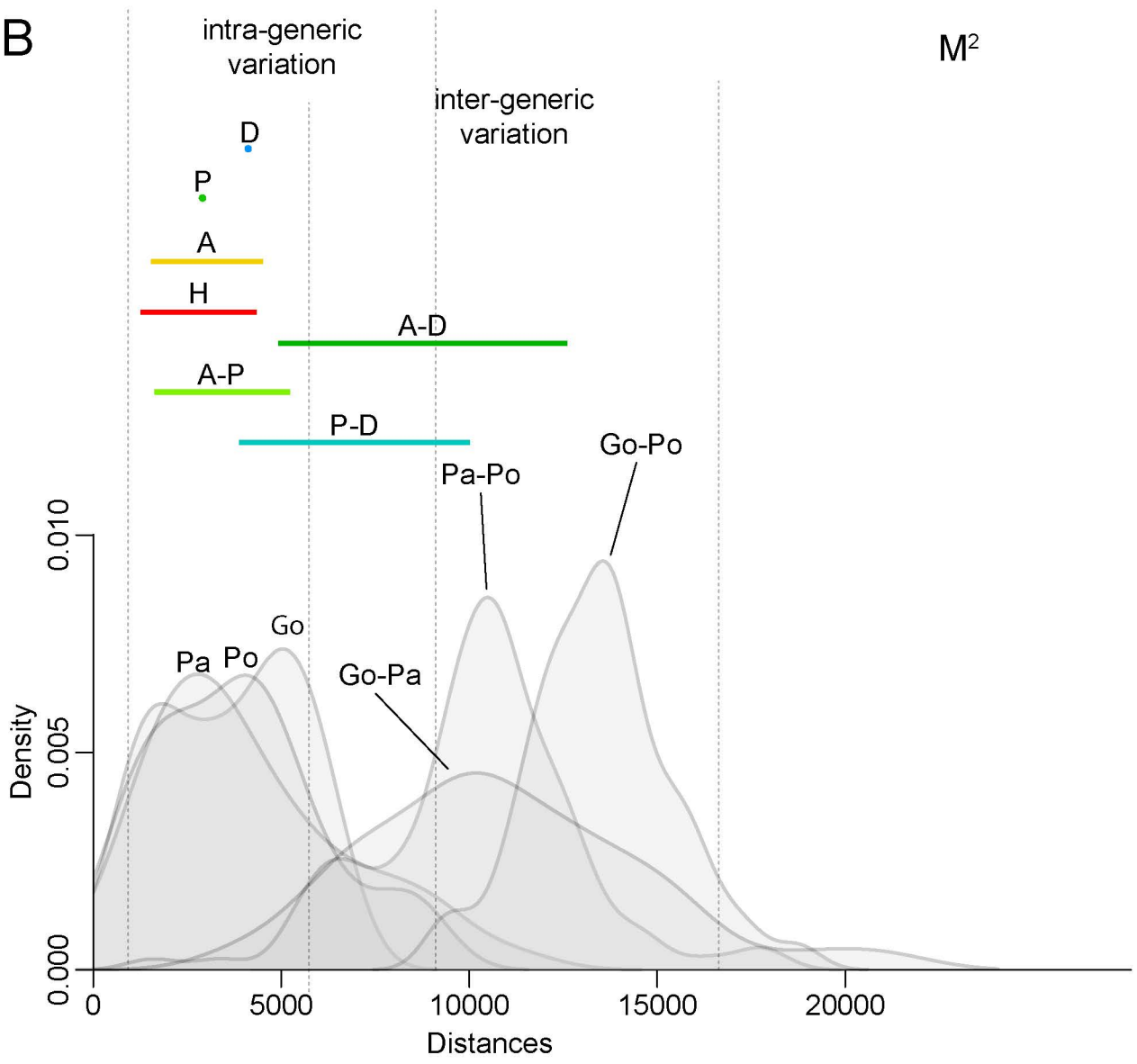
intra-generic variation
inter-generic variation
M2
D
P
A
H
A-D
A-P
P-D
Go-Po
Pa-Po
Go-Pa
Pa
Po
Go
Density
0.000
0.005
0.010
0
5000
10000
15000
20000
Distances

E

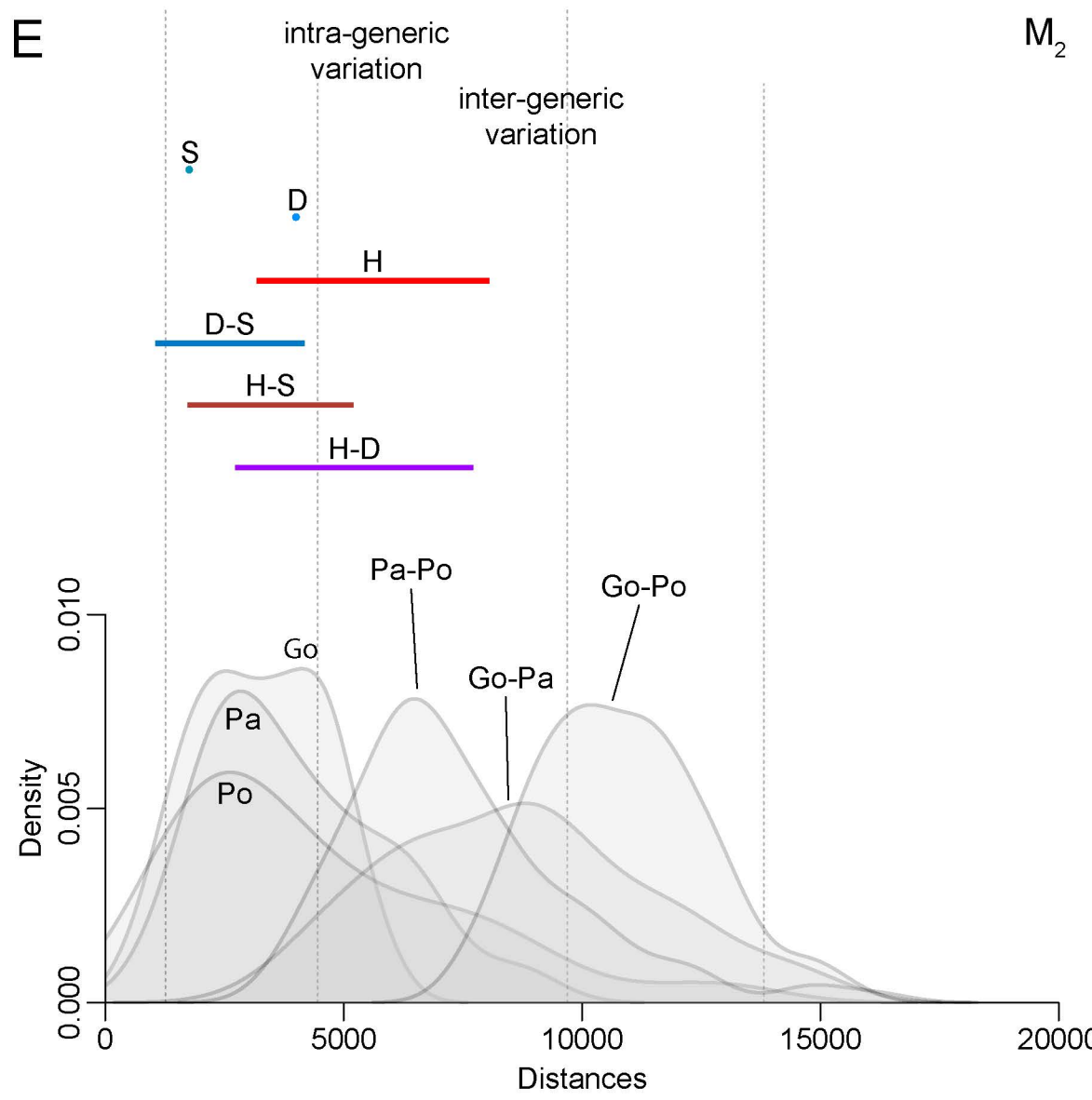
intra-generic variation
inter-generic variation
M2
S
D
H
D-S
H-S
H-D
Pa-Po
Go-Po
Go
Pa
Po
Go-Pa
Density
0.000
0.005
0.010
0
5000
10000
15000
20000
Distances

C

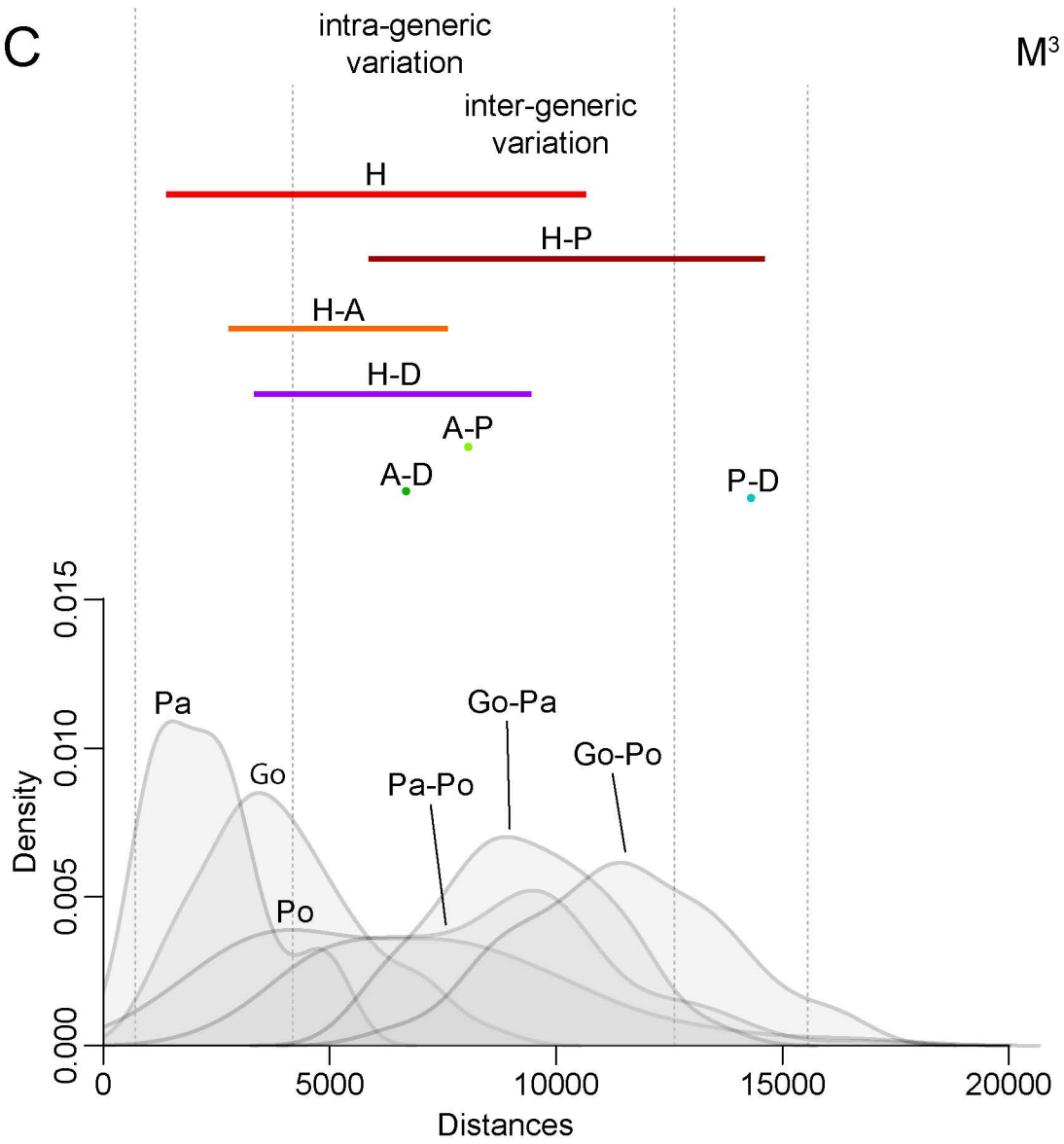
intra-generic variation
inter-generic variation
M3
H
H-P
H-A
H-D
A-P
A-D
P-D
Pa
Go
Po
Pa-Po
Go-Pa
Go-Po
Density
0.000
0.005
0.010
0.015
0
5000
10000
15000
20000
Distances

F

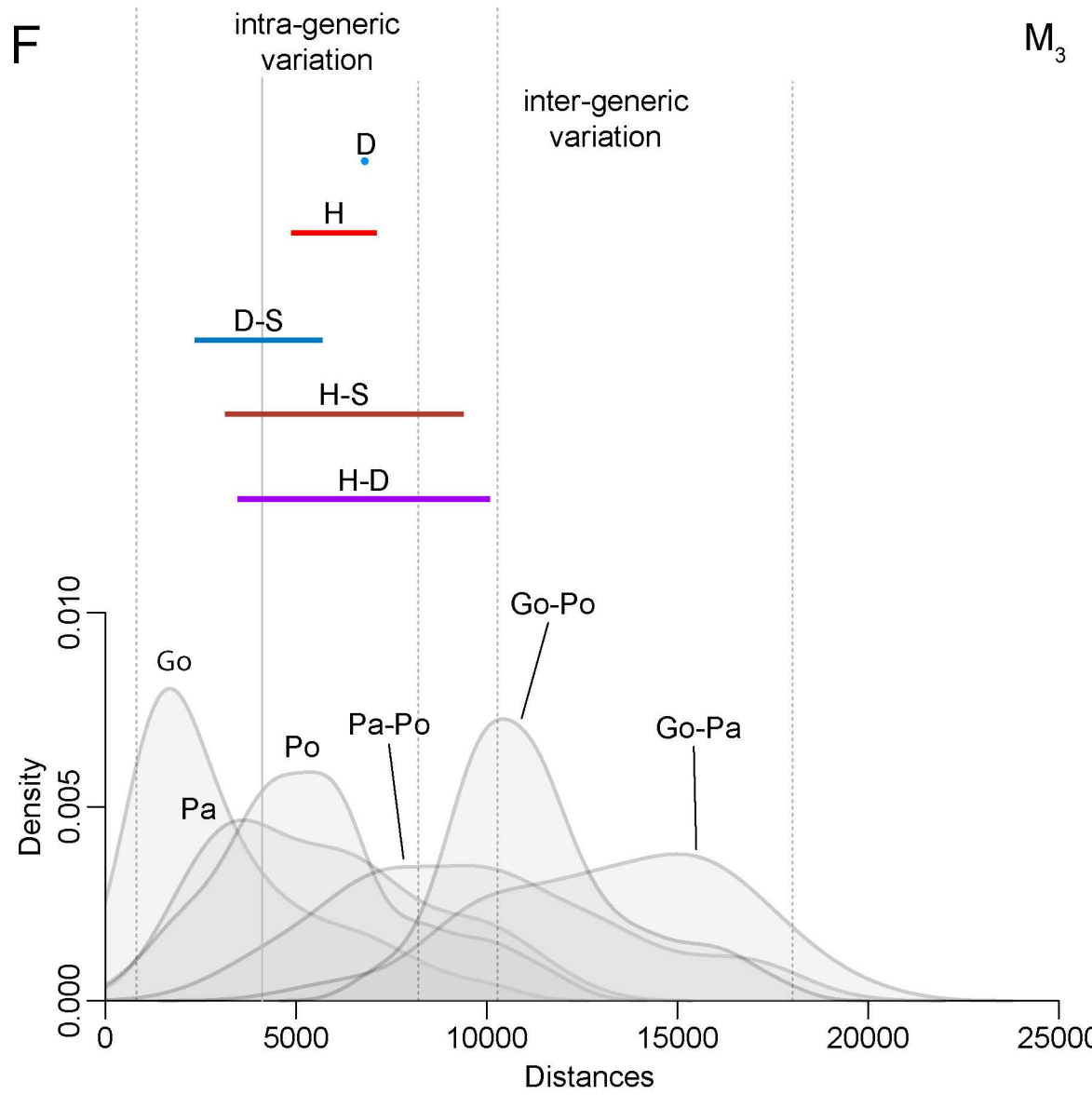
intra-generic variation
inter-generic variation
M3
D
H
D-S
H-S
H-D
Go-Po
Go
Pa-Po
Po
Go-Pa
Pa
Density
0.000
0.005
0.010
0
5000
10000
15000
20000
25000
Distances

Supplementary Online Material (SOM):

A reassessment of the distinctiveness of dryopithecine genera from the Iberian Miocene based on enamel-dentine junction geometric morphometric analyses

Clément Zanolli[a,*], Florian Bouchet[b], Josep Fortuny[b], Federico Bernardini[c,d], Claudio Tuniz[d], David M. Alba[b,*]

[a] *Univ. Bordeaux, CNRS, MCC, PACEA, UMR 5199, F-33600 Pessac, France*

[b] *Institut Català de Paleontologia Miquel Crusafont, Universitat Autònoma de Barcelona, Edifici ICTA-ICP, c/ Columnes s/n, Campus de la UAB, 08193 Cerdanyola del Vallès, Barcelona, Spain*

[c] *Department of Humanistic Studies, Università Ca'Foscari, Venezia, Italy*

[d] *Multidisciplinary Laboratory, 'Abdus Salam' International Centre for Theoretical Physics, Via Beirut 31, 34151 Trieste, Italy*

*Corresponding authors.

E-mail addresses: clement.zanolli@gmail.com (C. Zanolli); david.alba@icp.cat (D.M. Alba).

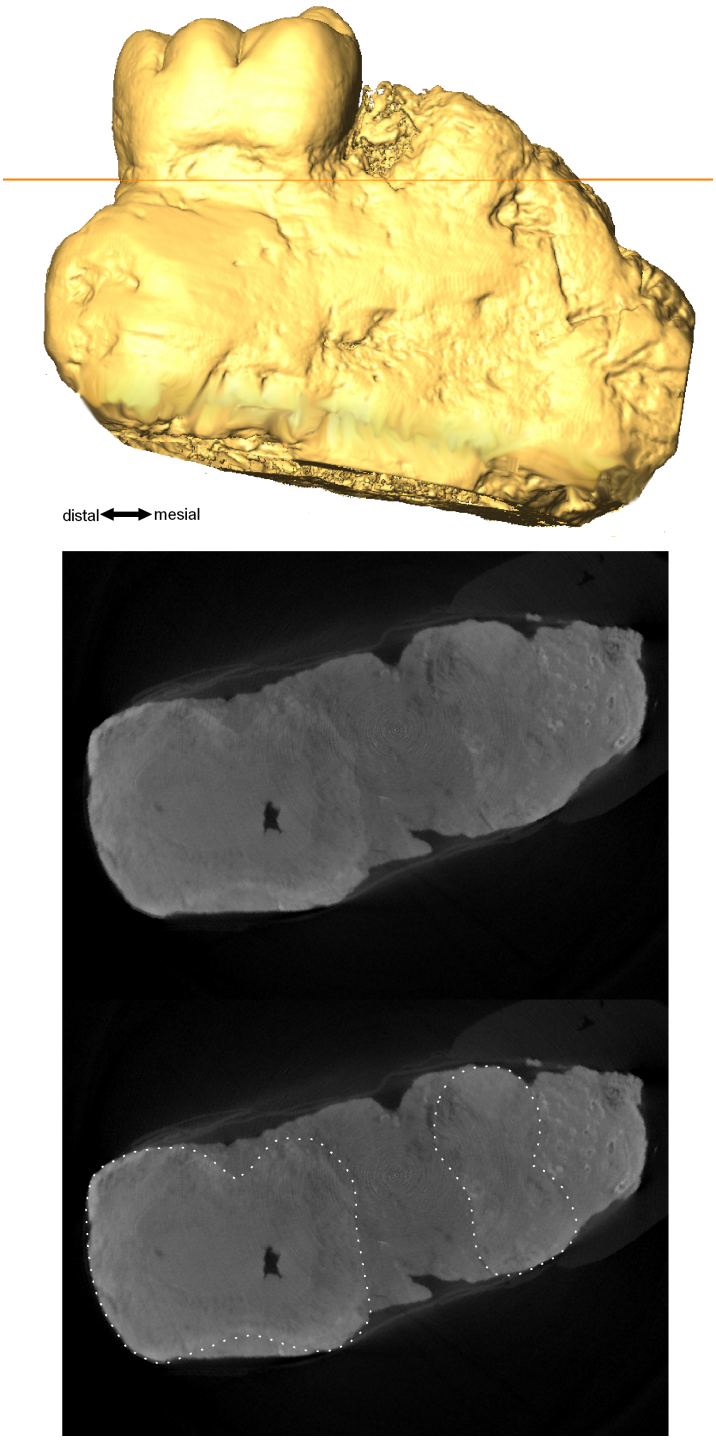

SOM Figure S1. Microtomographic section showing the roots of the IPS1816 molar and of the mesially-located tooth, more compatible with the morphology of a P_4 than of a M_1.

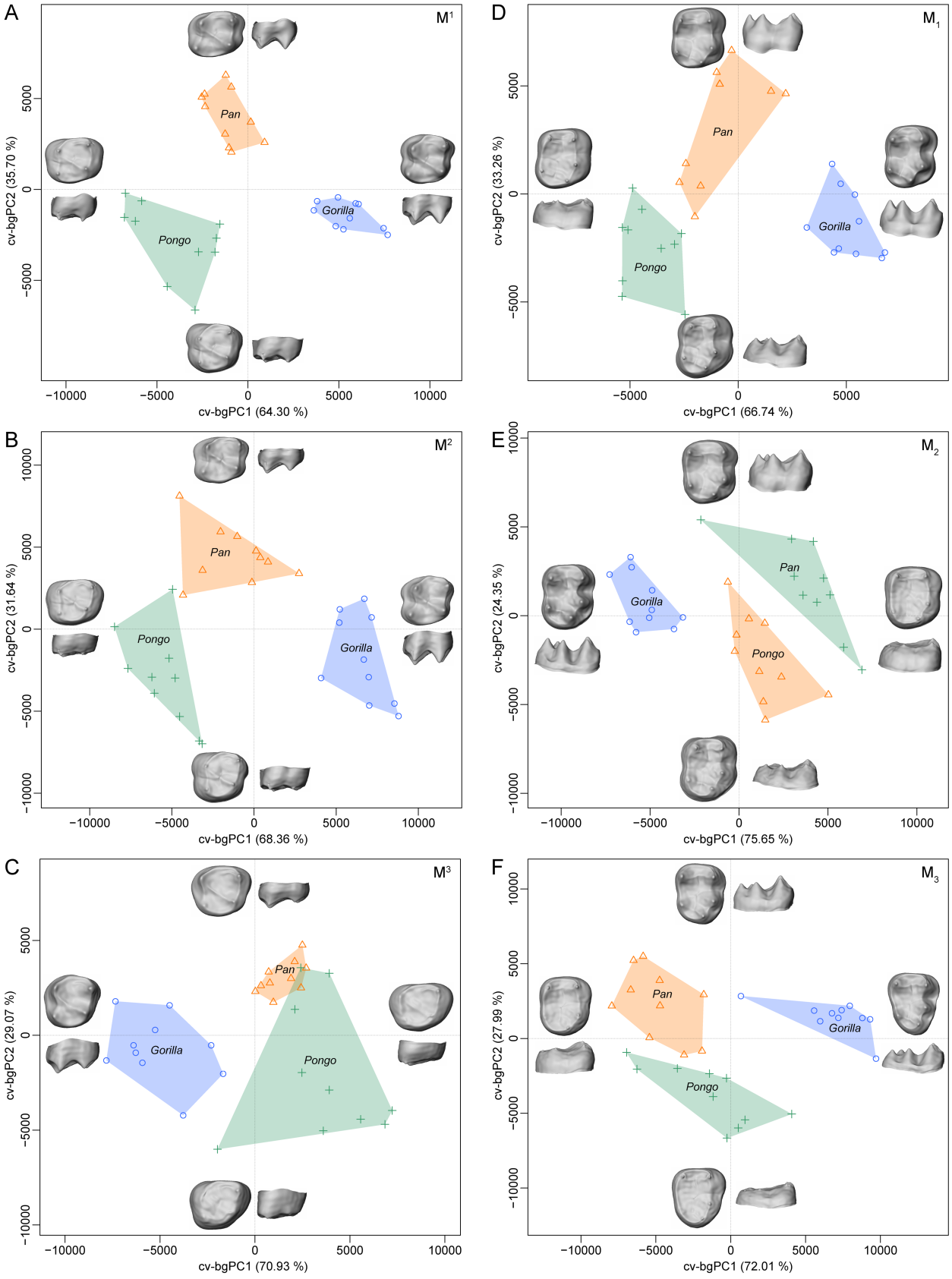
A
M1
Pan
Pongo
Gorilla
cv-bgPC2 (35.70 %)
cv-bgPC1 (64.30 %)
B
M2
Pan
Pongo
Gorilla
cv-bgPC2 (31.64 %)
cv-bgPC1 (68.36 %)
C
M3
Pan
Gorilla
Pongo
cv-bgPC2 (29.07 %)
cv-bgPC1 (70.93 %)
D
M1
Pan
Gorilla
Pongo
cv-bgPC2 (33.26 %)
cv-bgPC1 (66.74 %)
E
M2
Pan
Gorilla
Pongo
cv-bgPC2 (24.35 %)
cv-bgPC1 (75.65 %)
F
M3
Pan
Gorilla
Pongo
cv-bgPC2 (27.99 %)
cv-bgPC1 (72.01 %)

SOM Figure S2. Bivariate plot of the cross-validated between-group principal component 2 (cv-bgPC2) against the cross-validated between-group component 1 (cv-bgPC1) based on the diffeomorphic surface matching analyses of the enamel-dentine junction of the M^1 (A), M^2 (B), M^3 (C), M_1 (D), M_2 (E), and M_3 (F) of the Miocene dryopithecine genera compared with the extant great apes. The surfaces at the end of the axes illustrate the extreme shapes along each component.

SOM Table S1

Studied samples of Miocene hominoids.[a]

Catalog No.	Tooth	Provenance[b]	Age	Species	DOI	Reference
2004.HARLE.44	L M_2	SG	12.5–11.1 Ma	*Dryopithecus fontani*		Alba et al. (2020)
2004.HARLE.44	L M_3	SG	12.5–11.1 Ma	*Dryopithecus fontani*		Alba et al. (2020)
2004.HARLE.46	R M_1 or M_2	SG	12.5–11.1 Ma	*Dryopithecus fontani*		Alba et al. (2020)
2004.HARLE.47	R M_3	SG	12.5–11.1 Ma	*Dryopithecus fontani*		Alba et al. (2020)
IPS1772	L M^3	CLL1	9.7 Ma	*Hispanopithecus laietanus*	doi:10.17602/M2/M166178	Fortuny et al. (2021)
IPS1780	R M_2	CLL1	9.7 Ma	*Hispanopithecus laietanus*	doi:10.17602/M2/M166181	Fortuny et al. (2021)
IPS1797	R M_1	CLL1	9.7 Ma	*Hispanopithecus laietanus*	doi:10.17602/M2/M166312	Fortuny et al. (2021)
IPS1797	R M_2	CLL1	9.7 Ma	*Hispanopithecus laietanus*	doi:10.17602/M2/M166183	Fortuny et al. (2021)
IPS1802	R M_1	CLL1	9.7 Ma	*Hispanopithecus laietanus*	doi:10.17602/M2/M166314	Fortuny et al. (2021)
IPS1802	R M_2	CLL1	9.7 Ma	*Hispanopithecus laietanus*	doi:10.17602/M2/M166316	Fortuny et al. (2021)
IPS1802	R M_3	CLL1	9.7 Ma	*Hispanopithecus laietanus*	doi:10.17602/M2/M166185	Fortuny et al. (2021)
IPS1804	L M_2	LT1	9.5 Ma	*Hispanopithecus laietanus*	doi:10.17602/M2/M166187	Fortuny et al. (2021)
IPS1812	R M^3	CP1	10.4–10.0 Ma	*Hispanopithecus crusafonti*	doi:10.17602/M2/M166200	Fortuny et al. (2021)
IPS1814	R M^3	CP1	10.4–10.0 Ma	*Hispanopithecus crusafonti*	doi:10.17602/M2/M166375	Fortuny et al. (2021)
IPS1815	L M^1	CP1	10.4–10.0 Ma	*Hispanopithecus crusafonti*	doi:10.17602/M2/M166372	Fortuny et al. (2021)
IPS1816	R M_1	CP1	10.4–10.0 Ma	*Hispanopithecus crusafonti*	doi:10.17602/M2/M166227	Fortuny et al. (2021)
IPS1818	L M^1	CP1	10.4–10.0 Ma	*Hispanopithecus crusafonti*	doi:10.17602/M2/M166229	Fortuny et al. (2021)
IPS1820	L M^2	CP1	10.4–10.0 Ma	*Hispanopithecus crusafonti*	doi:10.17602/M2/M166230	Fortuny et al. (2021)
IPS1822	L M_3	CLL1	9.7 Ma	*Hispanopithecus laietanus*	doi:10.17602/M2/M166232	Fortuny et al. (2021)
IPS1826	L M_2	CV	12.0–11.9 Ma	*'Sivapithecus' occidentalis* species inquirenda	doi:10.17602/M2/M166233	Alba et al. (2020); Fortuny et al. (2021)
IPS1827	L M_3	CV	12.0–11.9 Ma	*'Sivapithecus' occidentalis* species inquirenda	doi:10.17602/M2/M166235	Alba et al. (2020); Fortuny et al. (2021)
IPS1844	R M^1	CLL1	9.7 Ma	*Hispanopithecus laietanus*	doi:10.17602/M2/M166318	Fortuny et al. (2021)
IPS18000.5	R M^2	CLL2	9.6 Ma	*Hispanopithecus laietanus*		Fortuny et al. (2021)
IPS18000.5	R M^3	CLL2	9.6 Ma	*Hispanopithecus laietanus*		Fortuny et al. (2021)
IPS21350	L M^1	ACM/BCV1	12.0 Ma	*Pieralopithecus catalaunicus*	doi:10.17602/M2/M166321	Fortuny et al. (2021)
IPS21350	L M^2	ACM/BCV1	12.0 Ma	*Pieralopithecus catalaunicus*	doi:10.17602/M2/M166323	Fortuny et al. (2021)

IPS21350	L M^3	ACM/BCV1	12.0 Ma	*Pieralopithecus catalaunicus*	doi:10.17602/M2/M166325	Fortuny et al. (2021)
IPS21350	R M^2	ACM/BCV1	12.0 Ma	*Pieralopithecus catalaunicus*	doi:10.17602/M2/M166327	Fortuny et al. (2021)
IPS35026	L M^1	ACM/C3-Ae	11.9 Ma	*Dryopithecus fontani*	doi:10.17602/M2/M166397	Fortuny et al. (2021)
IPS35026	L M^2	ACM/C3-Ae	11.9 Ma	*Dryopithecus fontani*	doi:10.17602/M2/M166393	Fortuny et al. (2021)
IPS35026	L M^3	ACM/C3-Ae	11.9 Ma	*Dryopithecus fontani*	doi:10.17602/M2/M166395	Fortuny et al. (2021)
IPS35027	R M^1	ACM/C1-E*	12.3–12.2 Ma	*Anoiapithecus brevirostris*	doi:10.17602/M2/M166403	Fortuny et al. (2021)
IPS35027	R M^2	ACM/C1-E*	12.3–12.2 Ma	*Anoiapithecus brevirostris*	doi:10.17602/M2/M166399	Fortuny et al. (2021)
IPS35027	L M^1	ACM/C1-E*	12.3–12.2 Ma	*Anoiapithecus brevirostris*	doi:10.17602/M2/M166405	Fortuny et al. (2021)
IPS35027	L M^2	ACM/C1-E*	12.4–12.3 Ma	*Anoiapithecus brevirostris*	doi:10.17602/M2/M166401	Fortuny et al. (2021)
IPS41734	R M_2	ACM/BCV4	11.9 Ma	"*Sivapithecus*" *occidentalis* species inquirenda	doi:10.17602/M2/M166406	Alba et al. (2020); Fortuny et al. (2021)
IPS43000	R M^1	ACM/C3-Aj	12.0 Ma	*Anoiapithecus brevirostris*	doi:10.17602/M2/M166408	Fortuny et al. (2021)
IPS43000	R M^2	ACM/C3-Aj	12.0 Ma	*Anoiapithecus brevirostris*	doi:10.17602/M2/M166410	Fortuny et al. (2021)
IPS43000	R M^3	ACM/C3-Aj	12.0 Ma	*Anoiapithecus brevirostris*	doi:10.17602/M2/M166412	Fortuny et al. (2021)
IPS43000	L M^1	ACM/C3-Aj	12.0 Ma	*Anoiapithecus brevirostris*	doi:10.17602/M2/M166414	Fortuny et al. (2021)
IPS43000	L M^2	ACM/C3-Aj	12.0 Ma	*Anoiapithecus brevirostris*	doi:10.17602/M2/M166416	Fortuny et al. (2021)
IPS43000	L M_1	ACM/C3-Aj	12.0 Ma	*Anoiapithecus brevirostris*	doi:10.17602/M2/M166418	Fortuny et al. (2021)
IPS43000	R M_1	ACM/C3-Aj	12.0 Ma	*Anoiapithecus brevirostris*	doi:10.17602/M2/M166422	Fortuny et al. (2021)
IPS58339	L M^2	CLL1	9.7 Ma	*Hispanopithecus laietanus*	doi:10.17602/M2/M166424	Fortuny et al. (2021)
IPS58340	L M^3	CLL1	9.7 Ma	*Hispanopithecus laietanus*	doi:10.17602/M2/M166426	Fortuny et al. (2021)
MGSB48486	R M^2	HP	11.3–11.0 Ma	*Dryopithecus fontani*	doi:10.17602/M2/M166460	Fortuny et al. (2021)
MGSB25314	L M_1	TF	10.4–10.0 Ma	*Hispanopithecus crusafonti*	doi:10.17602/M2/M166462	Fortuny et al. (2021)
MGSB25314	L M_2	TF	10.4–10.0 Ma	*Hispanopithecus crusafonti*	doi:10.17602/M2/M166472	Fortuny et al. (2021)
MGSB25314	L M_3	TF	10.4–10.0 Ma	*Hispanopithecus crusafonti*	doi:10.17602/M2/M166464	Fortuny et al. (2021)

Abbreviations: L = left; R = right; SG = Saint Gaudens; IPS = 'Institut de Paleontologia de Sabadell', former name of Institut Català de Paleontologia Miquel Crusafont; MGSB = Museu de Geologia del Seminari de Barcelona; ACM = local stratigraphic series of Abocador de Can Mata (els Hostalets de Pierola); C1 = Cell 1 (ACM sector); C3 = Cell 3 (ACM sector); BCV = Barranc de Can Vila (ACM sector); CLL = Can Llobateres (Sabadell); CP = Can Poncic (Sant Quirze); CV = Can Vila (els Hostalets de Pierola); HP = Hostalets de Pierola indet. (els Hostalets de Pierola); LT = La Tarumba (Viladecavalls); TF = Teuleria del Firal (Seu d'Urgell).

[a] Specimens highlighted in bold represent the holotype of the species.

[b] Acronyms in capital letters denote fossil sites, whereas numbers and other alphanumeric (in the case of ACM) denote localities within sites with multiple fossiliferous layers.

SOM Table S2

Comparative sample of extant great apes.

Specimen	Tooth	Sex	Species	DOI or ARK	Reference
CCEC-50001994	L M^1	F	*Gorilla gorilla*		ESRF Database (2021)
CCEC-50001994	R M^1	F	*Gorilla gorilla*		ESRF Database (2021)
MCZ 20089	R M^1	F	*Gorilla gorilla*	doi:10.17602/M2/M2945	MorphoSource Database (2021)
MCZ 37625	L M^1	F	*Gorilla gorilla*	doi:10.17602/M2/M2950	MorphoSource Database (2021)
MCZ 37625	R M^1	F	*Gorilla gorilla*	doi:10.17602/M2/M2950	MorphoSource Database (2021)
MCZ 49006	L M^1	F	*Gorilla gorilla*	doi:10.17602/M2/M2957	MorphoSource Database (2021)
MCZ 49006	R M^1	F	*Gorilla gorilla*	doi:10.17602/M2/M2957	MorphoSource Database (2021)
MHNT ZOO 2011.0.5	R M^1	?	*Gorilla* sp.		Braga et al. (2015)
MRAC 35274	L M^1	M	*Gorilla gorilla*		
MRAC 35274	R M^1	M	*Gorilla gorilla*		
CCEC-50001755	L M^1	M	*Pan troglodytes*		ESRF Database (2021)
CCEC-50001755	R M^1	M	*Pan troglodytes*		ESRF Database (2021)
CCEC-50001759	L M^1	?	*Pan troglodytes*		ESRF Database (2021)
CCEC-50001759	R M^1	?	*Pan troglodytes*		ESRF Database (2021)
CCEC-50001992	L M^1	?	*Pan troglodytes*		ESRF Database (2021)
MRAC 82032	R M^1	?	*Pan troglodytes*		
MRAC 84036	L M^1	M	*Pan paniscus*		
MRAC 84036	R M^1	M	*Pan paniscus*		
MRAC 88041	L M^1	?	*Pan troglodytes*		
MRAC 88041	R M^1	?	*Pan troglodytes*		
IPS10647	L M^1	F	*Pongo pygmaeus*		
IPS10647	R M^1	F	*Pongo pygmaeus*		
MCZ 37518	L M^1	F	*Pongo pygmaeus*	doi:10.17602/M2/M4613	MorphoSource Database (2021)

MCZ 37518	R M^1	F	*Pongo pygmaeus*	doi:10.17602/M2/M4613	MorphoSource Database (2021)
MHNB 2003.60	L M^1	?	*Pongo* sp.		
MHNB 2003.60	R M^1	?	*Pongo* sp.		
PACEA *Pongo*	L M^1	?	*Pongo* sp.		
PACEA *Pongo*	R M^1	?	*Pongo* sp.		
MZS 2625	L M^1	?	*Pongo* sp.		
MZS 2625	R M^1	?	*Pongo* sp.		
MCZ 20089	L M^2	F	*Gorilla gorilla*	doi:10.17602/M2/M2945	MorphoSource Database (2021)
MCZ 37264	L M^2	F	*Gorilla gorilla*	doi:10.17602/M2/M2949	MorphoSource Database (2021)
MCZ 37264	R M^2	F	*Gorilla gorilla*	doi:10.17602/M2/M2949	MorphoSource Database (2021)
MCZ 37266	R M^2	F	*Gorilla gorilla*	doi:10.17602/M2/M2952	MorphoSource Database (2021)
MCZ 37625	L M^2	F	*Gorilla gorilla*	doi:10.17602/M2/M2950	MorphoSource Database (2021)
MCZ 37625	R M^2	F	*Gorilla gorilla*	doi:10.17602/M2/M2950	MorphoSource Database (2021)
MCZ 46325	L M^2	F	*Gorilla gorilla*	doi:10.17602/M2/M2955	MorphoSource Database (2021)
MCZ 46325	R M^2	F	*Gorilla gorilla*	doi:10.17602/M2/M2955	MorphoSource Database (2021)
MCZ 49006	L M^2	F	*Gorilla gorilla*	doi:10.17602/M2/M2957	MorphoSource Database (2021)
MCZ 49006	R M^2	F	*Gorilla gorilla*	doi:10.17602/M2/M2957	MorphoSource Database (2021)
AMNH M-51204	L M^2	M	*Pan troglodytes*	ark:87602/m4/M21952	MorphoSource Database (2021)
AMNH M-167342	L M^2	M	*Pan troglodytes*	ark:87602/m4/M21967	MorphoSource Database (2021)
AMNH M-167342	R M^2	M	*Pan troglodytes*	ark:87602/m4/M21967	MorphoSource Database (2021)
IPS5698	L M^2	M	*Pan troglodytes*		Urciuoli et al. (2021)
IPS5698	R M^2	M	*Pan troglodytes*		Urciuoli et al. (2021)
MCZ 38018	L M^2	M	*Pan paniscus*	doi:10.17602/M2/M4399	MorphoSource Database (2021)
MCZ 38018	R M^2	M	*Pan paniscus*	doi:10.17602/M2/M4399	MorphoSource Database (2021)
MRAC 84036	L M^2	M	*Pan paniscus*		
MRAC 88041	L M^2	?	*Pan troglodytes*		
MRAC 88041	R M^2	?	*Pan troglodytes*		

IPS9031	L M^2	F	*Pongo* sp.		Urciuoli et al. (2021)
IPS9031	R M^2	F	*Pongo* sp.		Urciuoli et al. (2021)
IPS10647	L M^2	F	*Pongo* sp.		Urciuoli et al. (2021)
IPS10647	R M^2	F	*Pongo* sp.		Urciuoli et al. (2021)
MCZ 37519	R M^2	F	*Pongo pygmaeus*	doi:10.17602/M2/M4615	MorphoSource Database (2021)
MZS 2630	R M^2	?	*Pongo* sp.		
MZS 2632	L M^2	?	*Pongo* sp.		MorphoSource Database (2021)
MZS 2632	R M^2	?	*Pongo* sp.		MorphoSource Database (2021)
SMF 59146	L M^2	?	*Pongo abelii*		
MSNT *Pongo*	R M^2	?	*Pongo* sp.		
MCZ 14750	L M^3	F	*Gorilla gorilla*	doi:10.17602/M2/M2938	MorphoSource Database (2021)
MCZ 14750	R M^3	F	*Gorilla gorilla*	doi:10.17602/M2/M2938	MorphoSource Database (2021)
MCZ 26850	L M^3	F	*Gorilla gorilla*	doi:10.17602/M2/M2947	MorphoSource Database (2021)
MCZ 26850	R M^3	F	*Gorilla gorilla*	doi:10.17602/M2/M2947	MorphoSource Database (2021)
MCZ 37264	L M^3	F	*Gorilla gorilla*		MorphoSource Database (2021)
MCZ 37264	R M^3	F	*Gorilla gorilla*		MorphoSource Database (2021)
MCZ 37266	R M^3	F	*Gorilla gorilla*		MorphoSource Database (2021)
MCZ 38326	L M^3	F	*Gorilla gorilla*	doi:10.17602/M2/M2953	MorphoSource Database (2021)
MCZ 38326	R M^3	F	*Gorilla gorilla*	doi:10.17602/M2/M2953	MorphoSource Database (2021)
MCZ 46325	L M^3	F	*Gorilla gorilla*	doi:10.17602/M2/M2955	MorphoSource Database (2021)
AMNH M-51204	L M^3	M	*Pan troglodytes*	ark:87602/m4/M21952	MorphoSource Database (2021)
AMNH M-51204	R M^3	M	*Pan troglodytes*	ark:87602/m4/M21952	MorphoSource Database (2021)
AMNH M-167342	L M^3	M	*Pan troglodytes*	ark:87602/m4/M21967	MorphoSource Database (2021)
AMNH M-167342	R M^3	M	*Pan troglodytes*	ark:87602/m4/M21967	MorphoSource Database (2021)
AMNH M-167344	L M^3	M	*Pan troglodytes*	ark:87602/m4/M23480	MorphoSource Database (2021)
AMNH M-167344	R M^3	M	*Pan troglodytes*	ark:87602/m4/M23480	MorphoSource Database (2021)
IPS5698	L M^3	M	*Pan troglodytes*		Urciuoli et al. (2021)

IPS5698	R M^3	M	*Pan troglodytes*		Urciuoli et al. (2021)
MCZ 38018	L M^3	M	*Pan troglodytes*	doi:10.17602/M2/M4399	MorphoSource Database (2021)
MCZ 38018	R M^3	M	*Pan troglodytes*	doi:10.17602/M2/M4399	MorphoSource Database (2021)
IPS9031	L M^3	F	*Pongo* sp.		Urciuoli et al. (2021)
IPS9031	R M^3	F	*Pongo* sp.		Urciuoli et al. (2021)
IPS10647	L M^3	F	*Pongo* sp.		Urciuoli et al. (2021)
IPS10647	R M^3	F	*Pongo* sp.		Urciuoli et al. (2021)
MCZ 37519	R M^3	F	*Pongo pygmaeus*	doi:10.17602/M2/M4615	
MZS 2628	L M^3	?	*Pongo* sp.		
MZS 2630	R M^3	?	*Pongo* sp.		
MZS 2632	L M^3	?	*Pongo* sp.		
MZS 2632	R M^3	?	*Pongo* sp.		
MSNT *Pongo*	R M^3	?	*Pongo* sp.		
CCEC-50001994	L M_1	F	*Gorilla gorilla*		ESRF Database (2021)
CCEC-50001994	R M_1	F	*Gorilla gorilla*		ESRF Database (2021)
MCZ 37625	L M_1	F	*Gorilla gorilla*	doi:10.17602/M2/M2951	MorphoSource Database (2021)
MCZ 37625	R M_1	F	*Gorilla gorilla*	doi:10.17602/M2/M2951	MorphoSource Database (2021)
MCZ 49006	L M_1	F	*Gorilla gorilla*	doi:10.17602/M2/M2957	MorphoSource Database (2021)
MHNT ZOO 2011.0.2	L M_1	?	*Gorilla* sp.		Braga et al. (2015)
UdP M326	L M_1	?	*Gorilla sp.*		
MRAC RG 809	R M_1	?	*Gorilla gorilla*		
MRAC RG 996	R M_1	?	*Gorilla gorilla*		
MRAC RG 997	L M_1	?	*Gorilla gorilla*		
CCEC-50001755	L M_1	M	*Pan troglodytes*		ESRF Database (2021)
CCEC-50001759	L M_1	?	*Pan troglodytes*		ESRF Database (2021)
CCEC-50002604	L M_1	?	*Pan troglodytes*		ESRF Database (2021)

CCEC-50002604	R M_1	?	*Pan troglodytes*		ESRF Database (2021)
MCZ 46414	R M_1	F	*Pan troglodytes*	doi:10.17602/M2/M4386	MorphoSource Database (2021)
MCZ 46415	L M_1	F	*Pan troglodytes*	doi:10.17602/M2/M4385	MorphoSource Database (2021)
MCZ 46415	R M_1	F	*Pan troglodytes*	doi:10.17602/M2/M4385	MorphoSource Database (2021)
MHNB 2005.3234	R M_1	M	*Pan* sp.		
MNHN-ZM-AC-1950-257	L M_1	F	*Pan troglodytes*		
UdP	R M_1	?	*Pan* sp.		
IPH A1919 12	R M_1	?	*Pongo* sp.		
MHNB 2003.60	L M_1	?	*Pongo* sp.		
MHNB 2003.60	R M_1	?	*Pongo* sp.		
MHNB. 2003.119	L M_1	?	*Pongo* sp.		
PACEA *Pongo*	L M_1	?	*Pongo* sp.		
PACEA *Pongo*	R M_1	?	*Pongo* sp.		
UdP	L M_1	?	*Pongo* sp.		
MZS 2631	L M_1	?	*Pongo* sp.		
MZS 2631	R M_1	?	*Pongo* sp.		
UdP N278	L M_1	?	*Pongo* sp.		
AMNH M-167338	L M_2	M	*Gorilla gorilla*	ark:87602/m4/M21965	MorphoSource Database (2021)
AMNH M-167338	R M_2	M	*Gorilla gorilla*	ark:87602/m4/M21965	MorphoSource Database (2021)
MCZ 20089	L M_2	F	*Gorilla gorilla*	doi:10.17602/M2/M2946	MorphoSource Database (2021)
MCZ 20089	R M_2	F	*Gorilla gorilla*	doi:10.17602/M2/M2946	MorphoSource Database (2021)
MCZ 37264	L M_2	F	*Gorilla gorilla*	doi:10.17602/M2/M2949	MorphoSource Database (2021)
MCZ 37264	R M_2	F	*Gorilla gorilla*	doi:10.17602/M2/M2949	MorphoSource Database (2021)
MCZ 37265	L M_2	F	*Gorilla gorilla*	doi:10.17602/M2/M2951	MorphoSource Database (2021)
MCZ 46325	L M_2	F	*Gorilla gorilla*	doi:10.17602/M2/M2956	MorphoSource Database (2021)
MCZ 46325	R M_2	F	*Gorilla gorilla*	doi:10.17602/M2/M2956	MorphoSource Database (2021)

MCZ 49006	R M_2	F	*Gorilla gorilla*	doi:10.17602/M2/M2958	MorphoSource Database (2021)
AMNH M-167342	R M_2	M	*Pan troglodytes*	ark:87602/m4/M21967	MorphoSource Database (2021)
MCZ 23167	L M_2	F	*Pan troglodytes*	doi:10.17602/M2/M4390	MorphoSource Database (2021)
MCZ 23167	R M_2	F	*Pan troglodytes*	doi:10.17602/M2/M4390	MorphoSource Database (2021)
MHNB 2003.91	R M_2	?	*Pan* sp.		
MHNB 2003.92	L M_2	?	*Pan* sp.		
MHNB 2003.92	R M_2	?	*Pan* sp.		
MHNB 2003.95	R M_2	?	*Pan* sp.		
MHNB 2003.96	L M_2	?	*Pan* sp.		
MHNB 2005.3234	L M_2	M	*Pan* sp.		
UdP	R M_2	?	*Pan* sp.		
IPH A1919 12	R M_2	?	*Pongo* sp.		
SMF 2639	L M_2	?	*Pongo pygmaeus*		
SMF 2639	R M_2	?	*Pongo pygmaeus*		
SMF 16745	R M_2	?	*Pongo pygmaeus*		
SMF 59148	L M_2	?	*Pongo abelii*.		
SMF 59148	R M_2	?	*Pongo abelii*		
MCZ 37519	L M_2	F	*Pongo pygmaeus*	doi:10.17602/M2/M4616	MorphoSource Database (2021)
MCZ 37519	R M_2	F	*Pongo pygmaeus*	doi:10.17602/M2/M4616	MorphoSource Database (2021)
MCZ 50958	L M_2	F	*Pongo pygmaeus*	doi:10.17602/M2/M4612	MorphoSource Database (2021)
MCZ 50958	R M_2	F	*Pongo pygmaeus*	doi:10.17602/M2/M4612	MorphoSource Database (2021)
AMNH M-167338	L M_3	M	*Gorilla gorilla*	ark:87602/m4/M21965	MorphoSource Database (2021)
MCZ 17684	L M_3	F	*Gorilla gorilla*	doi:10.17602/M2/M2944	MorphoSource Database (2021)
MCZ 17684	R M_3	F	*Gorilla gorilla*	doi:10.17602/M2/M2944	MorphoSource Database (2021)
MCZ 26850	L M_3	F	*Gorilla gorilla*	doi:10.17602/M2/M2948	MorphoSource Database (2021)
MCZ 37264	L M_3	F	*Gorilla gorilla*	doi:10.17602/M2/M2949	MorphoSource Database (2021)

MCZ 37264	R M_3	F	*Gorilla gorilla*	doi:10.17602/M2/M2949	MorphoSource Database (2021)
MCZ 38326	L M_3	F	*Gorilla gorilla*	doi:10.17602/M2/M2954	MorphoSource Database (2021)
MCZ 38326	R M_3	F	*Gorilla gorilla*	doi:10.17602/M2/M2954	MorphoSource Database (2021)
MCZ 46325	L M_3	F	*Gorilla gorilla*	doi:10.17602/M2/M2955	MorphoSource Database (2021)
MCZ 46325	R M_3	F	*Gorilla gorilla*	doi:10.17602/M2/M2955	MorphoSource Database (2021)
AMNH M-167342	R M_3	M	*Pan troglodytes*	ark:87602/m4/M21967	MorphoSource Database (2021)
MCZ 6244	L M_3	M	*Pan troglodytes*	doi:10.17602/M2/M4394	MorphoSource Database (2021)
MCZ 6244	R M_3	M	*Pan troglodytes*	doi:10.17602/M2/M4394	MorphoSource Database (2021)
MCZ 15312	L M_3	F	*Pan troglodytes*	doi:10.17602/M2/M4391	MorphoSource Database (2021)
MCZ 15312	R M_3	F	*Pan troglodytes*	doi:10.17602/M2/M4391	MorphoSource Database (2021)
MCZ 23167	L M_3	F	*Pan troglodytes*	doi:10.17602/M2/M4390	MorphoSource Database (2021)
MCZ 23167	R M_3	F	*Pan troglodytes*	doi:10.17602/M2/M4390	MorphoSource Database (2021)
MCZ 26847	L M_3	F	*Pan troglodytes*	doi:10.17602/M2/M4389	MorphoSource Database (2021)
MHNB 2003.91	R M_3	?	*Pan* sp.		
MHNB 2003.92	R M_3	?	*Pan* sp.		
IPH A1919 12	R M_3	?	*Pongo* sp.		
MCZ 37518	R M_3	F	*Pongo pygmaeus*	doi:10.17602/M2/M4614	MorphoSource Database (2021)
MCZ 37519	L M_3	F	*Pongo pygmaeus*	doi:10.17602/M2/M4616	MorphoSource Database (2021)
MCZ 37519	R M_3	F	*Pongo pygmaeus*	doi:10.17602/M2/M4616	MorphoSource Database (2021)
MCZ 50958	L M_3	F	*Pongo pygmaeus*	doi:10.17602/M2/M4612	MorphoSource Database (2021)
MCZ 50958	R M_3	F	*Pongo pygmaeus*	doi:10.17602/M2/M4612	MorphoSource Database (2021)
SMF 16745	L M_3	?	*Pongo pygmaeus*		
SMF 59148	L M_3	?	*Pongo abelii*		
SMF 59148	R M_3	?	*Pongo abelii*		
MSNT *Pongo*	L M_3	?	*Pongo* sp.		

Abbreviations: CCEC = Centre de conservation et d'étude des collections of the Musée des Confluences; MCZ = Harvard Museum of Comparative Zoology; MHNT = Muséum d'Histoire Naturelle of Toulouse; MRAC = Musée royal de l'Afrique centrale of Tervuren; IPS = 'Institut de Paleontologia de Sabadell', former name of Institut Català de Paleontologia Miquel Crusafont; MNHB = Muséum d'Histoire naturelle of Bordeaux; PACEA = Laboratory PACEA of the University of Bordeaux; MZS = Musée Zoologique of Strasbourg; AMNH = American Museum of Natural History; SMF = 'Senckenberg Museum of Frankfurt', former name of Senckenberg Research Institute and Natural History Museum Frankfurt; MSNT = Museo di Storia Naturale of Trieste; UdP = Université de Poitiers; IPH = Institut de Paléontologie Humaine.

SOM Table S3

Results of the permutational analysis of variance testing the group structure in the raw data.[a]

Tooth	Groups compared	Raw data	
		r^2	*p*-value
M^1	GOR vs. PAN	0.32	**<0.01**
	GOR vs. PON	0.32	**<0.01**
	PAN vs. PON	0.24	**<0.01**
M^2	GOR vs. PAN	0.31	**<0.01**
	GOR vs. PON	0.40	**<0.01**
	PAN vs. PON	0.26	**<0.01**
M^3	GOR vs. PAN	0.24	**<0.01**
	GOR vs. PON	0.25	**<0.01**
	PAN vs. PON	0.16	**<0.01**
M_1	GOR vs. PAN	0.26	**<0.01**
	GOR vs. PON	0.38	**<0.01**
	PAN vs. PON	0.23	**<0.01**
M_2	GOR vs. PAN	0.24	**<0.01**
	GOR vs. PON	0.30	**<0.01**
	PAN vs. PON	0.14	**<0.01**
M_3	GOR vs. PAN	0.35	**<0.01**
	GOR vs. PON	0.31	**<0.01**
	PAN vs. PON	0.17	**0.01**

Abbreviations: GOR = *Gorilla*; PAN = *Pan*; PON = *Pongo*.

[a] Probabilities are shown after Holm correction and significant values are highlighted in bold.

SOM Table S4

Cross-validated bgPCA and CVA correct classifications for the comparative specimens (*n* = 10/genus) attributed to *Gorilla* (GOR), *Pan* (PAN), and *Pongo* (PON).

Tooth	GOR		PAN		PON		Overall accuracy	
	bgPCA	CVA	bgPCA	CVA	bgPCA	CVA	bgPCA	CVA
M^1	10 (100.0%)	10 (100.0%)	10 (100.0%)	10 (100.0%)	10 (100.0%)	10 (100.0%)	30/30 (100.0%)	30/30 (100.0%)
M^2	10 (100.0%)	10 (100.0%)	10 (100.0%)	9 (90.0%)	9 (90.0%)	10 (100.0%)	29/30 (96.7%)	29/30 (96.7%)
M^3	10 (100.0%)	10 (100.0%)	10 (100.0%)	10 (100.0%)	6 (60.0%)	8 (80.0%)	26/30 (86.7%)	28/30 (93.3%)
M_1	10 (100.0%)	10 (100.0%)	8 (80.0%)	10 (100.0%)	10 (100.0%)	10 (100.0%)	28/30 (93.3%)	30/30 (100.0%)
M_2	10 (100.0%)	10 (100.0%)	10 (100.0%)	10 (100.0%)	10 (100.0%)	10 (100.0%)	30/30 (100.0%)	30/30 (100.0%)
M_3	9 (90.0%)	10 (100.0%)	8 (80.0%)	10 (100.0%)	8 (80.0%)	10 (100.0%)	25/30 (83.3%)	30/30 (100.0%)

SOM References

Alba, D.M., Fortuny, J., Robles, J.M., Bernardini, F., Pérez de los Ríos, M., Tuniz, C., Moyà-Solà, S., Zanolli, C., 2020. A new dryopithecine mandibular fragment from the middle Miocene of Abocador de Can Mata and the taxonomic status of '*Sivapithecus' occidentalis* from Can Vila (Vallès-Penedès Basin, NE Iberian Peninsula). J. Hum. Evol. 145, 102790.

Braga, J., Loubes, J.M., Decouens, D., Dumoncel, J., Thackeray, J.F., Kahn, J.L., de Beed, F., Riberon, A., Hoffman, K., Balaresque, P., Gilissen, E., 2015. Disproportionate cochlear length in genus *Homo* shows a high phylogenetic signal during apes' hearing evolution. PLoS One 10, e0127780.

ESRF Database, 2021. European Synchrotron Radiation Facility Paleontological Microtomographic Database. http://paleo.esrf.eu.

Fortuny, J., Zanolli, C., Bernardini, F., Tuniz, C., Alba, D.M., 2021. Dryopithecine palaeobiodiversity in the Iberian Miocene revisited on the basis of molar endostructural morphology. Palaeontology 64, 531–554.

MorphoSource Database, 2021. MorphoSource Database. https://www.morphosource.org.

Urciuoli, A., Zanolli, C., Beaudet, A., Pina, M., Almécija, S., Moyà-Solà, S., Alba, D.M., 2021. A comparative analysis of the vestibular apparatus in *Epipliopithecus vindobonensis*: Phylogenetic implications. J. Hum. Evol. 151, 102930.